An assessment of equatorial Atlantic interannual variability in OMIP simulations

Arthur Prigent[1] and Riccardo Farneti[1]

[1]Earth System Physics, The Abdus Salam International Centre for Theoretical Physics (ICTP), Trieste, 34134, Italy

Correspondence: Arthur Prigent (aprigent@ictp.it)

Abstract. The eastern equatorial Atlantic (EEA) seasonal cycle and interannual variability strongly influence the climate of the surrounding continents. It is thus crucial that models used in both climate predictions and future climate projections are able to simulate them accurately. In that context, the EEA monthly climatology and interannual variability are evaluated over the period 1985-2004 in models participating to the Ocean Model Intercomparison Project Phases 1 and 2 (OMIP1 and OMIP2). The main difference between OMIP1 and OMIP2 simulations is their atmospheric forcing: CORE-II and JRA55-do, respectively. Monthly climatologies of the equatorial Atlantic zonal wind, sea level anomaly and sea surface temperature in OMIP1 and OMIP2 are comparable to reanalysis products. Yet, some discrepancies exist in both OMIP ensembles: the thermocline is too diffusive and there is a lack of cooling during the development of the Atlantic cold tongue. The EEA interannual sea surface temperature variability during May-June-July in the OMIP1 ensemble mean is found to be 51% larger (0.62 ± 0.04 °C) than the OMIP2 ensemble mean (0.41 ± 0.03 °C). Likewise, the May-June-July interannual sea surface height variability in the EEA is 33% larger in the OMIP1 ensemble mean (0.02 ± 0.002 m) than in the OMIP2 ensemble mean (0.015 ± 0.002 m). Sensitivity experiments demonstrate that the discrepancy in interannual sea surface temperature and sea surface height variabilities between OMIP1 and OMIP2 is mainly attributable to their wind forcing, and specifically to its variability. While the April-May-June zonal wind variability in the western equatorial Atlantic is similar in both forcing, the zonal wind variability peaks in April for JRA55-do and in May for CORE-II.

1 Introduction

The sea surface temperature (SST) in the equatorial Atlantic exhibits a marked seasonal cycle closely related to the seasonal displacement of the intertropical convergence zone (ITCZ). In March-April-May (MAM), highest temperatures are observed in the equatorial region (>27 °C) as the sun is positioned directly overhead, resulting in maximum incident solar radiation (Xie and Carton, 2004). In this season, the ICTZ is situated close to the equator leading to weak trade winds that cause a deep thermocline in the eastern equatorial Atlantic (EEA). As the year progresses the ITCZ migrates northward, and the southeasterly winds intensify. This shift leads to a shoaling of the thermocline, enhanced upwelling and vertical mixing as well as intensified evaporation in the EEA (Lübbecke et al., 2018). Consequently, from May to June, the Atlantic cold tongue (ACT) forms east of 20°W, persisting until September with SSTs below 25 °C. The initiation of the ACT and the West African

25 Monsoon (WAM) have been observed to be interconnected. In fact, delayed onsets of the ACT and WAM are associated with anomalously warm SSTs in the EEA (Brandt et al., 2011; Caniaux et al., 2011).

Every few years, the SST in the EEA experiences large deviations (>1.5 °C) from its climatology, resulting from the Atlantic Niño or Atlantic zonal mode (Servain et al., 1982; Zebiak, 1993; Keenlyside and Latif, 2007; Lübbecke et al., 2018). Atlantic Niños (Niñas) are characterised by warm (cold) SST anomalies developing in the ATL3 region (Zebiak (1993); 20°W-0°E,
30 3°S-3°N, indicated by the blue box in Figure 1). The ATL3 interannual SST variability denotes two peaks, one in May-June-July (MJJ), during the development of the ACT and driven by Atlantic Niños (Figure 1a), and another in November-December driven by the Atlantic Niños II (Okumura and Xie, 2006). The interannual SST variability in the EEA is phased-locked to the seasonal cycle, with maximum variability occurring in boreal summer when the thermocline is shallow and the surface-subsurface coupling is maximum (Keenlyside and Latif, 2007). The underlying dynamics of the Atlantic Niño bears some
35 resemblance to that observed during El Niño/Southern Oscillation in the Pacific ocean (Zebiak, 1993), involving a coupling between SST, zonal wind stress and ocean heat content as described by the Bjerknes feedback (BF; Bjerknes, 1969). The BF can be decomposed into three components: (BF1) the forcing of western equatorial Atlantic (ATL4; 40°W-20°W, 3°S-3°N; green box in Figure 1a) zonal wind anomalies by SST anomalies in the ATL3 region; (BF2) the forcing of thermocline depth anomalies in the ATL3 region by zonal wind anomalies in the ATL4; (BF3) the forcing of SST anomalies in the ATL3 by
40 local thermocline depth anomalies. All three BF components are active in the equatorial Atlantic although they are generally weaker and display a stronger seasonal modulation than those observed in the Pacific (Keenlyside and Latif, 2007; Burls et al., 2012; Lübbecke and McPhaden, 2017; Dippe et al., 2019). The study of Atlantic Niños is of particular importance as they have shown to influence the climate of the neighbouring continents (Hirst and Hastenrath, 1983; Folland et al., 1986; Nobre and Shukla, 1996), the El Niño/Southern Oscillation (Rodríguez-Fonseca et al., 2009), the Indian Monsoon (Kucharski et al.,
45 2008), and European climate (Cassou et al., 2005). Atlantic Niños may also drive equatorial Atlantic interannual chlorophyll-a concentration variability (Chenillat et al., 2021).

Despite substantial warm biases found in state-of-the-art coupled general circulation models (CGCM) in the EEA (Davey et al., 2002; Richter and Tokinaga, 2020; Farneti et al., 2022), CGCMs are still capable of reproducing the BF (Deppenmeier et al., 2016). A number of them manage to simulate realistic interannual SST variability within the ATL3 during boreal summer
50 (Figure 1b; see also Richter and Tokinaga, 2020). However, while the CGCM ensemble mean depicts too weak interannual SST variability in the EEA, it shows excessive interannual SST variability off the coasts of Angola and Namibia during boreal summer (Figure 1b). Prodhomme et al. (2019) showed, using Coupled Model Intercomparison Project (CMIP) phase 5 simulations, that the representation of the Atlantic Niño is strongly linked to the cold tongue development, highlighting the importance to accurately capture the seasonal evolution of the wind stress and SST in CGCMs. CGCMs have been extensively
55 evaluated in the tropical Atlantic region, serving as valuable tools for comprehending and predicting variability patterns (Crespo et al., 2022; Prigent et al., 2023a, b). To our knowledge, relatively little effort has been devoted to the simulation of interannual variability in ocean general circulation models (OGCMs) in the tropical Atlantic. Wen et al. (2017) analysed the response of tropical ocean simulations with two different surfaces forcings: the National Centers for Environmental Prediction/DOE reanalysis 2 (NCEP/DOE-R2; Kanamitsu et al., 2002) and the Climate Forecast System Reanalysis (CFSR; Saha et al., 2010).
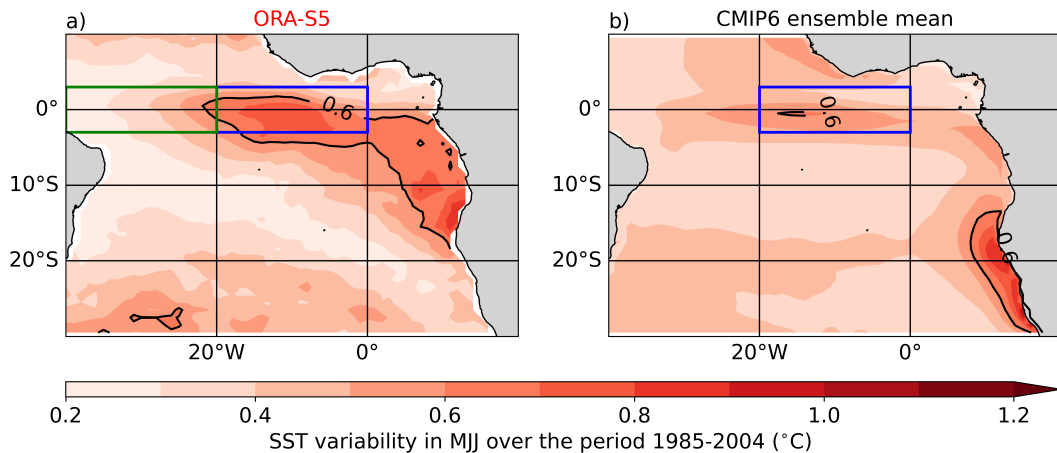
Figure 1. Interannual SST variability in the tropical Atlantic during MJJ. Standard deviation of the MJJ-averaged SST anomalies for (a) ORA-S5, (b) CMIP6 ensemble mean, spanning from January 1985 to December 2004. The CMIP6 ensemble is composed of 55 models listed in Supplementary Table S1. The blue and green boxes represent the ATL3 (20°W-0°E, 3°S-3°N) and ATL4 (40°W-20°W, 3°S-3°N) regions, respectively.

60   They found that the magnitude of the ocean temperature variability simulated using these two surface forcings was comparable in the tropical Pacific, however, they showed that using CFSR lead to some improvements in the tropical Atlantic, emphasising that the improvements in the tropical Atlantic were mainly attributable to differences in surface winds.

The Ocean Model Intercomparison Project (OMIP; Griffies et al., 2016) provides an ideal framework for evaluating the simulation of the interannual variability in the equatorial Atlantic by ocean models. The main objective of OMIPs is to provide

65   a framework for assessing, understanding and improving the ocean and sea-ice components of global climate models that contribute to the CMIP. OMIPs have used two atmospheric and river runoff datasets to force ocean sea-ice models. In OMIP phase 1 (OMIP1; Griffies et al., 2009), the Coordinated Ocean-ice Reference Experiments phase-II atmospheric state (CORE-II; Large and Yeager, 2009), mainly derived from the NCEP atmospheric reanalysis phase 1, was employed. In OMIP phase 2 (OMIP2; Griffies et al., 2016; Tsujino et al., 2020), the JRA-55 based surface dataset for driving ocean–sea-ice models

70   (JRA55-do; Tsujino et al., 2018) was used. In the present study we will address the following questions: how well do OMIP1 and OMIP2 ensembles simulate the monthly climatologies of equatorial Atlantic zonal winds, sea level anomalies (SLA) and SSTs? What are the differences in the interannual variability within the EEA between OMIP1 and OMIP2? Which component of the atmospheric forcing is responsible for these differences?

To address these questions we utilise various observational datasets, reanalysis products, and conduct sensitivity experiments,

75   all of which are detailed in section 2. We scrutinise the seasonal patterns of equatorial Atlantic zonal winds, SLAs and SSTs in section 3. Section 4 is dedicated to assessing the interannual SST, SSH and temperature variability within OMIP1 and OMIP2

ensembles. In section 5, we delve into the impact of wind forcing on the EEA interannual variability. Final conclusions along with discussions can be found in section 6.

2 Data and methods

2.1 Data

2.1.1 Reanalysis products and observational datasets

This study employs several reanalysis products with monthly temporal resolution, if not stated otherwise. Specifically, SST, sea surface height (SSH), zonal wind stress, and upper 200 m depth ocean potential temperature are taken from the Ocean Reanalysis System version 5 (ORA-S5; Zuo et al., 2019). ORA-S5 provides data at a horizontal resolution of $0.25°$ by $0.25°$ and spans the period from January 1958 to present day. ORA-S5 has 72 z-levels in the ocean. The Optimum Interpolation SST version 2 (OI-SST, Reynolds et al., 2002) is also used, it is available at a horizontal resolution of $1°$ by $1°$ over the period from December 1981 to January 2023. Additionally, zonal winds at 10 m height (U10) are obtained from the CORE-II atmospheric state (Large and Yeager, 2009), with a horizontal resolution of $2°$ by $2°$ and a temporal resolution of 6 hours encompassing the period from January 1948 to December 2009, and from the JRA55-do atmospheric forcing derived from the Japanese 55 years Reanalysis (Griffies et al., 2016; Tsujino et al., 2018), with a horizontal resolution of $0.5625° \times 0.5625°$ (~ 55 km $\times$ 55 km at the equator) and a temporal resolution of 3 hours spanning from January 1958 to December 2018. In addition to reanalysis products, zonal winds at 10 m height are taken from the Cross-Calibrated Multi-Platform version 2 (CCMP v2; Mears et al., 2019), providing data at a horizontal resolution of $0.25°$ by $0.25°$ and spanning from January 1988 to December 2017. To validate the SLA from the OMIP models, we compare it to the monthly mean gridded AVISO data version vDT2021 distributed by the Copernicus Climate Change Service (C3S, 2018), and available at a horizontal resolution of $0.25°$ by $0.25°$ spanning the period from January 1993 to present.

2.1.2 OMIP data

In this study, we assess how models participating in OMIP1 and OMIP2 simulate the equatorial Atlantic interannual variability. The OMIP1 protocol consists of five consecutive cycles of the 62-year-long CORE-II atmospheric state (Large and Yeager, 2009), whereas the OMIP2 protocol consists of six consecutive cycles of the 61-year-long JRA55-do forcing. The JRA55-do has a higher temporal resolution (3 hourly) and finer spatial resolution ($0.5625° \times 0.5625° \sim 55$ km $\times$ 55 km at the equator) than the CORE-II forcing (6 hourly and $2°$ by $2°$, respectively). Models participating in both OMIPs have used the same ocean model physics. For the purpose of analysis, we focused on the fifth and sixth cycle of OMIP1 and OMIP2, respectively, during a common period from January 1985 to December 2004, aligning with Farneti et al. (2022). All ocean models with a resolution finer than $1°$ by $1°$ and having all the variables needed for this study are listed in Table 1. Considered models were bi-linearly interpolated horizontally onto a regular $1°$ by $1°$ grid and vertically on the following depth levels: 6, 15, 25, 35, 45, 55, 65, 75, 85, 95, 105, 115, 125, 135, 145, 156.9, 178.4, 222.5, 303.1. The following variables were utilised in the analysis: SST

Table 1. OMIP1 models (0-6) and OMIP2 models (7-14) used in this study. The table indicates the model name, the ocean model used as well as the number of grid points in the longitudinal, latitudinal and vertical dimensions.

Num	Model name	Ocean model	Ocean resolution (nlon × nlat × nlevels)
0	CMCC-CM2-SR5	NEMO3.6	362 × 292 × 50
1	CMCC-ESM2	NEMO3.6	362 × 292 × 50
2	EC-Earth3	NEMO3.6	362 × 292 × 75
3	IPSL-CM6A-LR	NEMO-OPA	362 × 332 × 75
4	MIROC6	COCO4.9	360 × 256 × 63
5	MRI-ESM2-0	MRI.COM4.4	360 × 364 × 61
6	NorESM2-LM	MICOM	360 × 384 × 70
7	ACCESS-OM2	MOM5.1	360 × 300 × 50
8	ACCESS-OM2-025	MOM5.1	1440 × 1080 × 50
9	CMCC-CM2-HR4	NEMO3.6	1442 × 1051 × 50
10	CMCC-CM2-SR5	NEMO3.6	362 × 292 × 50
11	EC-Earth3	NEMO3.6	362 × 292 × 75
12	MIROC6	COCO4.9	360 × 256 × 63
13	MRI-ESM2-0	MRI.COM4.4	360 × 364 × 61
14	NorESM2-LM	MICOM	360 × 384 × 70

(variable name: TOS), SSH (variable name: ZOS), zonal wind stress (variable name: UAS), ocean temperature (variable name: THETAO), mixed layer depth (variable name: MLOTST), and net surface heat flux (variable name: HFDS).

2.1.3 CMIP6 data

All fifty five CMIP6 models from the variant r1i1p1f1 considered in Figure 1 are listed in Table S1. We use monthly mean outputs of SST (variable name: TOS) retrieved over the historical period from January 1985 to December 2004. Before analysis, CMIP6 models' outputs were bi-linearly interpolated on a common $1°$ by $1°$ regular grid.

2.1.4 Simulations with the GFDL-MOM5 model

We conducted several modelling experiments to complement the OMIP analyses. We employed the NOAA-GFDL Modular Ocean Model version 5 (MOM5; Griffies, 2012), which is a free-surface primitive equation model and uses a $z^\star$ rescaled geopotential coordinate.

First, we performed a control run (MOM5-LR) following the OMIP2 protocol (Griffies et al., 2016), running the MOM5 ocean model for six consecutive cycles of the 61-year-long JRA55-do forcing. The simulation was conducted at $1°$ resolution in the horizontal and with 50 vertical levels. In MOM5-LR, subgrid mesoscale processes are parameterized with the Gent-McWilliams skew-flux closure scheme (Gent and Mcwilliams, 1990; Gent et al., 1995; Griffies, 1998) and submesoscale eddy

Table 2. Table summarising the different configurations of the MOM5 experiments. The table indicates: the experiment name, the horizontal resolution, the number of vertical levels, the atmospheric forcing, and the wind forcing. In MOM5-LR-anom, the wind forcing is a synthetic reconstruction obtained from the JRA55-do monthly climatological mean and the CORE-II monthly anomalies from their climatology.

Name	Horizontal resolution	Number of vertical level	Atmospheric forcing	Wind forcing
MOM5-LR	$1° \times 1°$	50	JRA55-do	JRA55-do
MOM5-HR	$0.25° \times 0.25°$	50	JRA55-do	JRA55-do
MOM5-LR-anom	$1° \times 1°$	50	JRA55-do	JRA55-do clim + CORE-II anom

fluxes according to Fox-Kemper et al. (2008) and Fox-Kemper et al. (2011). Vertical mixing is represented with a K-profile parameterization (Large et al., 1994).

Next, we examined the influence of the wind forcing on the EEA interannual variability. An additional experiment, MOM5-LR-anom, mirrors the MOM5-LR configuration, with the exception that we repeated the sixth cycle by replacing the JRA55-do winds at 10 m height (U10 and V10) with a reconstructed wind field. The wind field used in MOM5-LR-anom is the sum of the JRA55-do monthly climatological mean plus the monthly anomalies from the climatological CORE-II winds. As turbulent fluxes of momentum, heat and moisture are derived through bulk formulae based on the near surface atmospheric state (including 10 m winds), all surfaces fluxes are expected to be affected by the reconstructed wind field. Also, although not energetically consistent with the other forcing variables, this configuration provides a sensitivity for the upper ocean response to the wind variability in the CORE-II forcing.

Finally, to assess the impact of the horizontal resolution on the simulation of interannual variability in the EEA, we conducted a MOM5-HR experiment following the OMIP2 protocol. MOM5-HR has a similar configuration to MOM5-LR, but its horizontal resolution is refined to $0.25°$ by $0.25°$ and the parameterization for mesoscale eddy fluxes is turned off. As for OMIP2 and MOM5-LR, we analysed the sixth cycle of MOM5-HR. In supplementary Text S1 we have evaluated the outputs of MOM5-LR and MOM5-HR simulations against ORA-S5, focusing on the equatorial Atlantic Ocean mean-state, monthly climatology and interannual temperature variability. This comparison shows that even though MOM5-LR and MOM5-HR feature some biases, both simulations are able to capture reasonably well the tropical Atlantic mean-state, monthly climatology as well as the upper 200 m temperature variability. MOM5 experiments and their main characteristics are summarised in Table 2.

2.2 Methodology

2.2.1 Definition of anomalies

We compare the EEA interannual variability simulated by the OMIP1 ensemble mean to the OMIP2 ensemble mean over a 20-year period spanning from January 1985 to December 2004. Throughout this paper, prior to all analysis, the linear trend is removed pointwise to each dataset. Monthly-mean anomalies are computed by subtracting the climatological monthly-mean seasonal cycle derived over the study period. The boreal summer interannual variability is quantified as the standard deviation of the MJJ-averaged anomalies.

2.2.2 Thermocline depth, mixed layer depth and sea level anomaly definitions

The mean depth of the thermocline is defined as the depth of the maximum vertical temperature gradient (dT/dz). SSH anomalies are used as a proxy for thermocline-depth variations. Mixed layer depth (MLD) is determined as the ocean depth at which the potential density σ_θ has increased by 0.03 kg·m^{-3} relative to the top model level value (Griffies et al., 2016). A discussion on the method and its implications in defining MLD in OMIP models can be found in Treguier et al. (2023). The MLD, dT/dz and corresponding depth of the maximum dT/dz are shown for each OMIP model and sensitivity experiments in Figure S1. Sea level anomaly (SLA) is defined as the pointwise difference between the SSH and the mean sea surface, with the mean sea surface calculated as the SSH averaged of the period January 1985 to December 2004. The equatorial Atlantic thermocline tilt is defined as the difference of the depth of the maximum dT/dz between the ATL4 and ATL3 regions.

2.2.3 Bjerknes feedback and thermal damping

The three components of the Bjerknes feedback (BF) are assessed as follows. The first component (BF1) is the linear regression of ATL4-averaged zonal wind stress anomalies in MJJ on ATL3-averaged SST anomalies in MJJ. The second component (BF2) is the linear regression of ATL3-averaged SSH anomalies in MJJ on ATL4-averaged zonal wind stress anomalies in MJJ. The third component (BF3) is the linear regression of ATL3-averaged SST anomalies in MJJ on ATL3-averaged SSH anomalies in MJJ. Additionally, the thermal damping is quantified as the linear regression of ATL3-averaged net heat flux anomalies in MJJ on ATL3-averaged SST anomalies in MJJ.

3 Comparison of the OMIP1 and OMIP2 equatorial Atlantic monthly climatologies

Accurately simulating the equatorial Atlantic wind, SLA and SST monthly climatologies in ocean models is crucial for the good representation of the EEA interannual SST variability (Prodhomme et al., 2019). Therefore, in this section we compare the OMIP1 and OMIP2 monthly climatological means of the equatorial Atlantic (40°W-10°E; 3°S-3°S) zonal winds, SLAs and SSTs to reanalysis products and observational datasets. A comparison to the Prediction and Research Moored Array in the Tropical Atlantic (PIRATA; Servain et al., 1998; Bourlès et al., 2008) at the equatorial moorings of 35°W, 23°W, 10°W, and 0°E can be found in Supplementary Text S2.

The monthly climatology of the zonal wind in the western equatorial Atlantic is dominated by an annual cycle with maximum easterly winds in September-October-November (SON) and minimum easterlies in MAM (Figure 2a). Meanwhile, the EEA zonal wind exhibits a semiannual cycle (Figure 2a) with maxima in January-February-March and SON. Both CORE-II (Figure 2b) and JRA55-do (Figure 2c) surface forcings closely mirror the observed monthly climatology of the zonal wind in the equatorial Atlantic. In the ATL4 region (Figure 2d), CORE-II and JRA55-do zonal winds are stronger than those of CCMP v2 throughout the year.

Next, we analyse the seasonal cycle of the SLA, where negative (positive) SLA indicates a shoaling (deepening) of the thermocline. Consistent with the strong link between western equatorial Atlantic zonal winds and the thermocline (Philander

Table 3. Table summarising key values allowing for the comparison of OMIP1 and OMIP2 ensemble means to ORA-S5 in the equatorial Atlantic, over the period from January 1985 to December 2004. Values in parenthesis are for JAS.

	ORA-S5/CCMP v2	OMIP1/CORE-II	OMIP2/JRA55-do
SLA 40°W-30°W SON minus MAM (m)	0.096	0.070 ± 0.008	0.050 ± 0.01
ATL3-averaged SLA in JJA (m)	-0.037	-0.028 ± 0.007	-0.029 ± 0.007
ATL3-averaged SST MAM (JAS) (°C)	28.52 (24.79)	28.51 ± 0.07 (25.31 ± 0.12)	28.63 ± 0.06 (25.34 ± 0.17)
Equatorial Atlantic U10 MAM (JAS) (m·s^{-1})	-1.91 (-2.24)	-1.89 (-2.76)	-1.99 (-2.27)
Equatorial tilt MAM (JAS) (m)	23.30 (44.45)	30.50 ± 3.52 (47.29 ± 3.49)	35.44 ± 5.61 (44.80 ± 3.93)
ATL3 upper 25 m temperature MAM (JAS) (°C)	28.44 (24.67)	28.38 ± 0.07 (25.22 ± 0.15)	28.42 ± 0.12 (25.25 ± 0.19)
ATL3-averaged MLD MAM (JAS) (m)	18.87 (26.26)	16.23 ± 1.45 (23.43 ± 2.94)	13.52 ± 3.36 (25.60 ± 5.69)
ATL3-averaged distance between Z20 and Z24 MAM (JAS) (m)	16.08 (23.23)	34.54 (31.94)	34.65 (30.21)

and Pacanowski, 1986), the seasonal cycle of the SLA depicts an annual cycle in the west (Figure 2e). In the east, a semiannual cycle appear in the SLA. Brandt et al. (2016) showed that the equatorial Atlantic seasonal cycle of SLA is driven by resonance modes associated with the second and fourth baroclinic modes at semiannual and annual frequencies, respectively. In the western equatorial Atlantic, the thermocline reaches its shallowest point during MAM and this signal progresses eastward, reaching 10°W by July. In SON, the thermocline is deep in the west and the signal also propagates eastward, but its propagation is faster. These eastward propagating SLA signals can be understood in terms of linear dynamics and are essentially explained by the first four baroclinic modes (Ding et al., 2009). Both the OMIP1 (Figure 2f) and OMIP2 (Figure 2g) ensemble means exhibit patterns similar to ORA-S5. In comparison to ORA-S5, the amplitude of the annual cycle in the western equatorial Atlantic is too weak in both OMIP ensembles (Table 3). However, relative to the OMIP2 ensemble mean, the annual cycle of the SLA in the western equatorial Atlantic is 40% larger in the OMIP1 ensemble mean. In the ATL3 region (Figure 2h) the shoaling of the thermocline in JJA, as indicated by the negative SLA, is about 30% too weak in both OMIP ensembles in comparison to ORA-S5 (Table 3).

The shoaling of the thermocline depth from MAM to JAS in the ATL3 region (Figure 2h) is closely related to the rapid decrease in SST (Figure 2i). In ORA-S5, the ATL3-averaged SST decreases from 28.52 °C in MAM to 24.79 °C in JAS, with a cooling of 3.73 °C (Table 3). In comparison to ORA-S5, both OMIP ensemble means (Figures 2j, k) generate a weaker cooling in the ATL3 region (3.19 ± 0.1 °C for OMIP1 and 3.29 ± 0.15 °C for OMIP2, Figure 2l) from MAM to JAS. It is noteworthy that the difference in cooling between the OMIP1 and OMIP2 ensemble means is mainly due to slightly warmer ATL3 SSTs in MAM for OMIP2 compared to OMIP1.

As the monthly climatology of the equatorial Atlantic SST is strongly influenced by subsurface conditions, we examined the upper 200 m ocean temperature during both MAM and JAS (Figure 3). During MAM (Figure 3a), the equatorial Atlantic easterly winds (40°W-10°E; 3°S-3°N) are relatively weak, measuring 1.91 m·s^{-1} in CCMP v2. Consequently, the thermocline exhibits a small tilt of 23.30 m, with the upper 25 m in the ATL3 region having a temperature of 28.44 °C. Notably, the

200 ATL3-averaged MLD is located at 18.87 m. We note that the vertical temperature gradient is pronounced in this region, with the distance between the 20 °C and 24 °C isotherms measuring 16.08 m. In JAS (Figure 3b), the equatorial Atlantic easterlies intensify to 2.24 m·s^{-1}, leading to a steeper thermocline with a tilt of 44.45 m and an increased slope of the isotherms between 20°W and 0°E. The upper 25 m in the ATL3 experiences a strong cooling, with a temperature of 24.67 °C, while the MLD deepens to 26.26 m.

205 Comparing the above values to the OMIP ensemble means (Table 3), we observe that the upper 200 m temperature sections in both MAM (Figures 3c, e) and JAS (Figures 3d, f) align closely with ORA-S5. However, some differences are listed next. In MAM (Figures 3c, e), the CORE-II (JRA55-do) easterlies in the equatorial Atlantic are slightly weaker (stronger) than CCMP v2 and the tilt of the thermocline is overestimated in both OMIP ensembles. The upper 25 m temperature in the ATL3 region is well captured by the OMIP1 and OMIP2 ensemble means but in both ensembles the MLD is too shallow (Table 3). Relative to

210 ORA-S5, both OMIP ensembles feature a too diffusive thermocline as indicated by the large distance between the 20 °C and 24 °C isotherms in the ATL3 region (Table 3). In JAS (Figure 3d, f), the equatorial Atlantic easterlies are overestimated in both ensembles, however, the tilt of the thermocline in the OMIP ensembles is close to the one from ORA-S5 (Table 3). The upper 25 m temperature from the OMIP ensemble means in the ATL3 is not cooling as much as in ORA-S5 (Table 3). Finally, the deepening of the ATL3-averaged MLD is better represented in the OMIP2 ensemble than in the OMIP1 ensemble (Table 3).

215 To summarise this section and answer the first question raised in the introduction, we find that the OMIP1 and OMIP2 ensemble means closely replicate the monthly climatologies of equatorial Atlantic zonal winds, SSTs, SLAs and upper 200 m ocean temperatures when compared to ORA-S5 and CCMP v2. Nonetheless, we highlight some discrepancies relative to ORA-S5: (1) the seasonal shoaling of the thermocline in JJA is about 30% weaker in both OMIP ensemble means, (2) both OMIP ensemble means exhibit a too diffusive thermocline; (3) the cooling of the SST and upper 25 m ocean temperature from MAM

220 to JAS in the ATL3 is less pronounced in the OMIP ensemble means.

4 Comparison of OMIP1 and OMIP2 equatorial Atlantic interannual variabilities

The interannual variability in the equatorial Atlantic exhibits a pronounced seasonality (Keenlyside and Latif, 2007; Lübbecke et al., 2018). Specifically, high interannual zonal wind variability in CCMP v2 in the western equatorial Atlantic occurs from 40°W to 20°W during April-May-June (Figure 4a) and from 20°W to 15°W in March and April. As OMIP1 and OMIP2

225 models are forced by the CORE-II and JRA55-do 10 m winds, respectively, we compare them to CCMP v2. The CORE-II zonal wind forcing displays a similar pattern to CCMP v2 from 40°W to 20°W but with weaker interannual variability (Figure 4b). The JRA55-do forcing also exhibits a similar pattern of interannual zonal wind variability but underestimates it in April-May-June (Figure 4c). Additionally, the JRA55-do forcing (Figure 4c) reveals high zonal wind variability between 10°W and 10°E in January and February, which is not as prominent in CCMP v2 (Figure 4a) and absent in the CORE-II forcing (Figure

230 4b). Quantitatively, the standard deviation of AMJ-averaged U10 anomalies in the ATL4 region is 0.80 m·s^{-1} for CCMP v2 over the period from January 1988 to December 2004 and 0.70 m·s^{-1} and 0.68 m·s^{-1} for CORE-II and JRA55-do over the period from January 1985 to December 2004, respectively. The ATL4-averaged monthly climatological standard deviation of

the U10 anomalies (Figure 4d) reveals that the peak zonal wind variability is in May for CORE-II and in April for JRA55-do and CCMP v2.

235   Typically, sudden relaxation (intensification) of the Trade winds in the western equatorial Atlantic can trigger interannual downwelling (upwelling) equatorial Kelvin waves (Illig et al., 2004). While propagating eastward along the equatorial wave guide, these waves generate thermocline-depth variations which can be observed in the SSH anomalies. In the following, we compare the equatorial Atlantic interannual SSH variability in OMIP1 and OMIP2 ensemble means to ORA-S5. In ORA-S5, two peaks of interannual SSH variability are observed during boreal summer, one between 40°W and 35°W and another

240   between 20°W and 0°E (Figure 4e). Additionally, ORA-S5 exhibits high interannual SSH variability in November-December in the EEA (Figure 4e). The interannual SSH variability in the ATL3 region is too strong (weak) in the OMIP1 (OMIP2) ensemble mean compared to ORA-S5 (Figure 4f, g, h). In numbers, the OMIP1 (OMIP2) ensemble mean ATL3-averaged interannual SSH variability in MJJ is 0.02 ± 0.002 m (0.015 ± 0.002 m), while it is 0.019 m in ORA-S5 (Figure 4h). The anomaly correlation coefficients and root-mean-square errors between OMIP1 and OMIP2 ensemble means with AVISO SLA,

245   evaluated over the period January 1993 to December 2004, are shown in Figures S2a-d. These figures show high correlation (>0.75, Figures S2a, b) and low root-mean-square error (<0.01 m, Figures S2c, d) in the EEA for both OMIP ensemble means, indicating a high fidelity of the OMIP ensembles with AVISO. To further illustrate that, we show the timeseries depicting ATL3-averaged SSH anomalies for AVISO, OMIP1, and OMIP2 ensemble means in Figure S2e. Despite robust correlations between both OMIP ensembles and AVISO (0.78), evaluated over the period from January 1993 to December 2004, the amplitude of

250   the monthly mean SSH anomalies is larger in OMIP1 compared to OMIP2. This indicates that thermocline depth variations are larger in the OMIP1 ensemble mean compared to the OMIP2 ensemble mean.

    Finally, we compare the equatorial Atlantic interannual SST variability from the OMIP1 and OMIP2 ensemble means to ORA-S5. ORA-S5 displays two peaks of interannual SST variability in the ATL3 region, one in MJJ and another in November-December (Figure 4i). Both OMIP ensemble means exhibit a similar pattern to ORA-S5. However, relative to ORA-S5, the

255   OMIP1 (OMIP2) ensemble mean overestimates (underestimates) the MJJ interannual SST variability in the EEA (Figures 4j, k). In numbers, the standard deviation of the MJJ-averaged SST anomalies in the ATL3 region is 0.62 ± 0.04 °C, 0.41 ± 0.03 °C and 0.59 °C for the OMIP1 and OMIP2 ensemble means and ORA-S5, respectively. The equatorial Atlantic interannual SST variability in MJJ is systematically larger in OMIP1 ensemble members than in OMIP2 ensemble members (Figure S3). The anomaly correlation coefficients and root-mean-square errors between OMIP1 and OMIP2 simulations with OI-SST,

260   evaluated over the period January 1985 to December 2004, are shown in Figures S4a-d. In comparison to the tropical Atlantic ocean, the EEA and southeastern tropical Atlantic display the lowest anomaly correlation and greatest root-mean-square errors across both OMIP1 and OMIP2 ensembles. This indicates that these regions exhibit the most pronounce biases between both OMIP ensembles and OI-SST. Nevertheless, it is important to highlight that despite these differences, the anomaly correlation coefficient is high (≈0.8, Figures S4a, b) and the root mean-square error is low (<0.5 °C, Figures S4c, d). To elaborate on this

265   point we present the timeseries depicting the ATL3-averaged SST anomalies for OI-SST, OMIP1 and OMIP2 ensemble means in Figure S4e. Both OMIP1 and OMIP2 ensemble means are highly correlated to OI-SST with Pearson correlation coefficients

of 0.79 and 0.80, respectively. However, the ATL3-averaged SST anomalies in the OMIP1 ensemble mean are in general larger than in the OMIP2 ensemble mean.

Ocean-atmosphere interactions are key drivers of the interannual SST variability within the EEA (Jouanno et al., 2017). To delve into this, we examined the various components of the Bjerknes feedback and thermal damping in ORA-S5, along with the ensemble means of OMIP1 and OMIP2 (Figure 5) over the period January 1985 to December 2004. The first component of the Bjerknes feedback is not discussed given that in a forced ocean model simulation, there is no response of the western equatorial Atlantic winds to the SST anomalies in the eastern equatorial Atlantic. In comparison to ORA-S5, for which the BF2 (Figure 5a) amounts to 1.79 m·(N·m^{-2})$^{-1}$, the OMIP1 (OMIP2) ensemble overestimates (underestimates) it with a slope of 1.96 $\pm$ 0.22 m·(N·m^{-2})$^{-1}$ (1.63 $\pm$ 0.30 m·(N·m^{-2})$^{-1}$). Regarding the BF3 (Figure 5b), it equals to 26.51 °C·m^{-1} for ORA-S5 and to 28.62 $\pm$ 2.42 °C·m^{-1} and 25.60 $\pm$ 1.67 °C·m^{-1} for the OMIP1 and OMIP2 ensembles, respectively. Hence, the subsurface-surface coupling is more pronounced in the OMIP1 ensemble mean than in the OMIP2 ensemble mean. Lastly, the thermal damping is assessed (Figure 5c). While ORA-S5 depicts a strong thermal damping (-21.58 W·m^{-2}·°C^{-1}) both OMIP ensembles underestimate it, with slopes of -12.47 $\pm$ 1.74 W·m^{-2}·°C^{-1} and -10.48 $\pm$ 2.5 W·m^{-2}·°C^{-1} for the OMIP1 and OMIP2 ensembles, respectively.

The contrast between the interannual variability of the equatorial Atlantic in the OMIP1 and OMIP2 ensemble means extends beyond the surface, as illustrated by the upper 200 m temperature variability in MJJ (Figure 6). In ORA-S5 (Figure 6a), two maxima of interannual temperature variability are observed in MJJ, one between 40°W and 30°W and another between 20°W and 0°E within $\pm$ 10 m range around the mean thermocline. The standard deviation of the ORA-S5 equatorial Atlantic SSH anomalies in MJJ mirrors the upper 200 m interannual temperature variability. The high interannual temperature variability in the western equatorial Atlantic is situated at a depth of 90 m, making it too deep to reach the MLD and, hence, affect the SST. In contrast, the maximum temperature variability in the EEA is located at 50 m depth, closer to the MLD, with an average of 1.28 °C for ORA-S5 when considering the ATL3 region and a $\pm$ 10 m range around the mean thermocline. The MJJ interannual temperature variability in the equatorial Atlantic for the OMIP ensemble means (Figure 6b, c) exhibits a similar pattern to ORA-S5 but with generally weaker interannual temperature variability. For both OMIP ensembles, the MJJ equatorial Atlantic interannual SSH variability mirrors the upper 200 m interannual temperature variability. The standard deviation of the MJJ-averaged temperature anomalies within $\pm$ 10 m of the mean thermocline for the ATL3 region is 0.78 $\pm$ 0.06 °C and 0.58 $\pm$ 0.07 °C for the OMIP1 and OMIP2 ensembles, respectively. The upper 200 m interannual temperature variability in the EEA during MJJ is systematically larger in OMIP1 ensemble members compared to OMIP2 ensemble members as shown in Figure S5. Given that both OMIP ensemble means exhibit a similar vertical temperature gradient during boreal summer within $\pm$ 10 m of the mean thermocline in the ATL3 region, amounting to -0.15 $\pm$ 0.001 °C·m^{-1}, it can be inferred that the disparities in the equatorial Atlantic interannual temperature variability are primarily driven by larger fluctuations in the thermocline depth. In contrast, the boreal summer vertical temperature gradient for ORA-S5 within $\pm$ 10 m of the mean thermocline in the ATL3 region is -0.25 °C·m^{-1}, which can account for its substantially higher subsurface temperature variability.

In response to the second question raised in the introduction, we showed that during the period January 1985 to December 2004, the OMIP1 ensemble exhibits about 51% (34%) greater boreal summer interannual SST (temperature) variability in

the ATL3 region compared to the OMIP2 ensemble. Over the same period and relative to the OMIP2 ensemble, the OMIP1 ensemble has about 33% greater interannual SSH variability in MJJ in the ATL3 region. When contrasting the two ensembles, the OMIP1 ensemble displays a stronger BF2 and BF3, which could account for the larger interannual SST variability. However, the thermal damping is more prominent in the OMIP1 ensemble than in the OMIP2 ensemble. In the next section, we investigate the impact of the CORE-II and JRA55-do wind forcings on the EEA interannual variability.

5 Influence of the wind forcing on the equatorial Atlantic interannual variability

Wind forcing is an important driver for the equatorial Atlantic mean-state, seasonal cycle and interannual variability (Richter et al., 2012; Wahl et al., 2011). Wen et al. (2017) investigated the response of tropical ocean simulations to NCEP/DOE-R2 and CFSR surface fluxes and, using sensitivity experiments with the GFDL MOM version 4p1 (Griffies, 2009), they found that prescribing CFSR surface fluxes instead of NCEP/DOE-R2 surface fluxes was significantly improving the simulation of the SST and SSH variabilities in the tropical Atlantic ocean. In the following, we aim to examine the hypothesis that the different equatorial Atlantic interannual variabilities observed in the OMIP ensemble means are a direct consequence of the discrepancies in wind forcing. A comparison of the CORE-II and JRA55-do reanalyses to other reanalysis products can be found in supplementary Text S3. To investigate this, we employ two simulations, namely MOM5-LR and MOM5-LR-anom, as described in section 2.1.4 and compared in Figure 7.

Both MOM5-LR (Figure 7a) and MOM5-LR-anom (Figure 7b) depict high boreal summer interannual SST variability within the ATL3 region. Yet, the MOM5-LR-anom simulation exhibits a larger interannual SST variability, amounting to 0.62 °C, in contrast to 0.42 °C for MOM5-LR. This implies that solely replacing JRA55-do monthly wind anomalies with CORE-II monthly wind anomalies results in a 48% increase in the EEA interannual SST variability. The equatorial Atlantic SSH variability in boreal summer also depicts an increase in MOM5-LR-anom (Figure 7d) relative to MOM5-LR (Figure 7c). Furthermore, this increase is not limited to the surface, as it is also reflected in the upper 200 m interannual temperature variability during boreal summer. Specifically, the MJJ interannual temperature variability within a ± 10 m range around the mean thermocline is 0.49 °C for MOM5-LR (Figure 7e) and 0.74 °C for MOM5-LR-anom (Figure 7f). Hence, using CORE-II monthly wind anomalies leads to a 51% increase in boreal summer interannual temperature variability in the ATL3 region and within ±10 m of the mean thermocline.

The impact of the wind forcing on the equatorial Atlantic interannual variability is further examined in Figure 8. In comparison to MOM5-LR (Figure 8a), MOM5-LR-anom (Figure 8b) exhibits a similar pattern of equatorial Atlantic interannual SSH variability, albeit with a larger magnitude. Quantitatively, the standard deviation of MJJ-averaged SSH anomalies in the ATL3 region amounts to 0.015 m for MOM5-LR and 0.020 m for MOM5-LR-anom. Furthermore, there seems to be a shift of about one month of the interannual SSH variability in the EEA when comparing Figures 8a and 8b. The monthly climatological standard deviation of the ATL3-averaged SSH anomalies (Figure 8c) shows that even though MOM5-LR and MOM5-LR-anom both peaks in June, the interannual SSH variability is stronger in May in MOM5-LR than in MOM5-LR-anom and the opposite in July. This temporal shift of about one month in the EEA interannual SSH variability could be related to the different peaks

in zonal wind variability in the ATL4 region between JRA55-do (April) and CORE-II (May). As previously discussed, we also find increased interannual SST variability in MOM5-LR-anom (Figure 8e) relative to MOM5-LR (Figure 8d). As for the ATL3 interannual SSH variability, a shift of about one month is also observed in the interannual SST variability when comparing MOM5-LR to MOM5-LR-anom (Figure 8f).

This section allowed us to answer the last question raised in the introduction. Namely, we have shown that the surface forcing, and in particular the wind variability, has a significant impact on the equatorial Atlantic interannual variability. Indeed, replacing the JRA55-do monthly wind anomalies by the CORE-II monthly wind anomalies results in a substantial increase in ATL3 interannual SST (48%), SSH (33%) and temperature (51%) variability during MJJ, rising from 0.42 °C, 0.015 m, and 0.49 °C for MOM5-LR to 0.62 °C, 0.020 m, and 0.74 °C for MOM5-LR-anom.

6 Conclusions and discussions

6.1 Conclusions

In this study, we have compared the monthly climatologies of equatorial Atlantic zonal wind, SLA, and SST from the OMIP1 and OMIP2 ensemble means to ORA-S5. Furthermore, we examined the equatorial Atlantic interannual variability within the OMIP models. Finally, we delved into the causes behind the distinct equatorial Atlantic interannual variabilities during boreal summer in OMIP1 and OMIP2 ensembles using sensitivity experiments. We have shown that over the period from January 1985 to December 2004:

- The climatological patterns of the equatorial Atlantic zonal wind, SLA, SST, and ocean temperature in OMIP1 and OMIP2 ensemble means resemble those in ORA-S5. However, some discrepancies are evident: the annual cycle of the SLA in the western equatorial Atlantic is too weak in both OMIP ensemble means, but the OMIP1 ensemble mean annual cycle of the SLA in the western equatorial Atlantic is about 40% larger than the one of the OMIP2 ensemble mean; the seasonal shoaling of the thermocline in the ATL3 region during JJA is about 30% too weak in the OMIP ensembles in comparison to ORA-S5; both OMIP ensembles have a too diffusive thermocline; the seasonal cooling of SST from MAM to JAS is insufficient in both OMIP ensembles (Figure 2).

- In the ATL3 region during boreal summer, the OMIP1 ensemble mean depicts a 51% greater interannual SST variability and a 34% larger interannual temperature variability at the thermocline level compared to the OMIP2 ensemble mean (Figure 9a).

- In boreal summer, both OMIP ensembles exhibit a comparable magnitude of dT/dz in the ATL3 region (Figure 9b). This suggests that, relative to the OMIP2 ensemble, heightened interannual SST and temperature variability in the OMIP1 ensemble cannot be attributed to differences in the magnitude of dT/dz.

- In boreal summer, the equatorial Atlantic thermocline tilt within OMIP models varies between 24 m and 39 m, while it reaches 30 m in the case of ORA-S5 (Figure 9c). No correlation between the thermocline tilt and the ATL3 interannual

SST variability is observed in OMIP models. It is worth noting that both MOM5-LR and MOM5-LR-anom exhibit a similar thermocline tilt, suggesting that the increased ATL3 interannual SST variability in MOM5-LR-anom is not attributable to a change in the thermocline tilt (Figure 9c).

- During AMJ, the zonal wind stress variability in the western equatorial Atlantic is slightly more pronounced in the OMIP1 ensemble mean compared to the OMIP2 ensemble mean. This difference may have played a role in the heightened interannual SST variability observed in ATL3 within the OMIP1 ensemble mean (as illustrated in Figure 9d). It is important to stress that the peak in ATL4 zonal wind variability occurs in April for the JRA55-do forcing and in May for the CORE-II forcing.

- Replacing the JRA55-do monthly wind anomalies for the CORE-II montlhy wind anomalies results in a 48% increase in ATL3 boreal summer interannual SST variability and a 51% increase in interannual temperature variability at the thermocline level, as depicted in Figure 9a. This underscores the critical role of interannual anomalies in the wind forcing in accurately simulating the equatorial Atlantic interannual variability within ocean models. It is worth noting that, in comparison to MOM5-LR, the magnitude of dT/dz in MOM5-LR-anom remains unchanged (Figure 9b).

- In boreal summer, the interannual SSH variability in the ATL3 region is about 33% greater in the OMIP1 ensemble mean compared to the OMIP2 ensemble mean (Figure 9e). Sensitivity experiments reveal that this change in ATL3 interannual SSH variability from the OMIP1 to the OMIP2 ensemble is mainly attributed to wind anomalies from the CORE-II forcing. Indeed, when comparing MOM5-LR to MOM5-LR-anom, the interannual SSH variability in the ATL3 region during boreal summer is heightened by 33%, as depicted in Figures 8 and 9f.

In summary, this study has shown, by comparing the OMIP1 and OMIP2 ensembles and by using sensitivity experiments, that seemingly minor uncertainties in the atmospheric forcing can lead to notable discrepancies in the simulated equatorial Atlantic interannual variability. For the equatorial Atlantic, we have shown that the interannual variability in ocean models is particularly sensitive to the wind forcing, in line with results from Wen et al. (2017).

6.2 Discussion

It could be argued that changes in ocean model physics from OMIP1 to OMIP2 could also have lead to discrepancies in the simulation of the interannual variability in the equatorial Atlantic. However, models participating in both OMIPs have used the same ocean model physics. Hence, discrepancies in the interannual variability in the EEA should be rooted in the atmospheric forcing. The simulation of the EEA interannual variability by ocean models may be influenced by several factors other than the wind forcing. Beyond the zonal and meridional winds, the forcing from CORE-II and JRA55-do includes shortwave and longwave heat fluxes, precipitation, river runoff, air temperature at 2 m and evaporation. However, their relative impact on the equatorial Atlantic interannual variability has not been investigated in this study and would require further model experiments and analysis.

Another factor potentially impacting on the simulation of the EEA is the ocean horizontal resolution. Model pairs such as ACCESS-OM2 and ACCESS-OM2-025, MOM5-LR and MOM5-HR, as well as CMCC-CM2-HR4 and CMCC-CM2-SR5, were compared to each other. Each model pair has the same number of vertical levels but they differ in their horizontal resolution, going from coarse ($1°\times1°$) to refined ($0.25°\times0.25°$). This comparison, based only on three model pairs, suggests that increasing the ocean horizontal resolution does not lead to consistent changes in the equatorial Atlantic mean-state and interannual SST variability in boreal summer (Figure 9). One notable change is the increase of the vertical ocean temperature gradient and subsurface temperature variability in boreal summer when comparing MOM5-LR to MOM5-HR (Figure 9b). However, this change is not observed in the other two model pairs. A larger number of model pairs would be required to properly assess the impact of horizontal resolution, and ideally also vertical resolution, on stratification biases. Finally, we note that both OMIP1 and OMIP2 ensembles are largely biased towards Eulerian vertical coordinate models, whereas a larger representation of models making use of Lagrangian vertical coordinates, or generalized vertical coordinates using the vertical Lagrangian-remap method (Griffies et al., 2020), such as MOM6 (Adcroft et al., 2019) and HYCOM (Bleck, 2002), could be extremely beneficial to the ocean modelling community.

To conclude, our study has underscored the importance of the wind forcing in modelling the interannual variability of the equatorial Atlantic. As a consequence, it is imperative to sustain and enhance wind observations in the tropical Atlantic in order to improve the quality of the reanalysis products in the region. We note that Taboada et al. (2019) conducted a comparative study of different wind reanalysis products and highlighted the lack of agreement among them in the tropics. Our results suggest that even though the monthly climatology of the equatorial Atlantic winds is relatively well captured by reanalysis datasets, their interannual variability needs more validation in the tropical Atlantic.

Finally, the use of JRA55-do forcing (Tsujino et al., 2018) within OGCMs seems to improve the simulation of SST variability in eddy-rich regions like the Gulf Stream, Kuroshio, Malvinas and Agulhas currents as well as in eastern boundary upwelling systems (Figure 10), probably also due to its higher temporal and spatial resolution compared to the CORE-II atmospheric state (Large and Yeager, 2009). However, the use of the JRA55-do atmospheric forcing results in a weak SST variability not only in the equatorial Atlantic (Figure 4) but also in the equatorial Pacific (Figure 10d). Due to its disproportionate role in the global climate at interannual and longer variabilities, further studies should focus on assessing the equatorial Pacific as represented by OMIP1 and OMIP2 models.

Code availability.

The MOM numerical ocean model version 5 is available from https://github.com/mom-ocean/MOM5. The scripts to reproduce the figures of the manuscript are available upon request to the corresponding author.

Data availability.

The ORA-S5 data is publicly available at the link: https://cds.climate.copernicus.eu/cdsapp#!/dataset/reanalysis-oras5?tab= form. The OI-SST data is publicly available at the link: https://psl.noaa.gov/data/gridded/data.noaa.oisst.v2.html. The CCMP v2 data is publicly available at the following link: https://apdrc.soest.hawaii.edu/erddap/griddap/hawaii_soest_3387_f2e3_ e359.html. The AVISO SLA was retrieved at the following link: https://cds.climate.copernicus.eu/cdsapp#!/dataset/10.24381/ cds.4c328c78?tab=overview. The OMIP1 and OMIP2 model output data were downloaded at the following link: https:// esgf-data.dkrz.de/projects/esgf-dkrz/. The CORE-II forcing is available at the following link: https://data1.gfdl.noaa.gov/nomads/ forms/core/COREv2.html. The JRA55-do forcing is available at the following link: https://climate.mri-jma.go.jp/pub/ocean/ JRA55-do/. The MOM5-LR, MOM5-LR-anom, and MOM5-HR datasets used in this study can be retrieved from Farneti (2024).
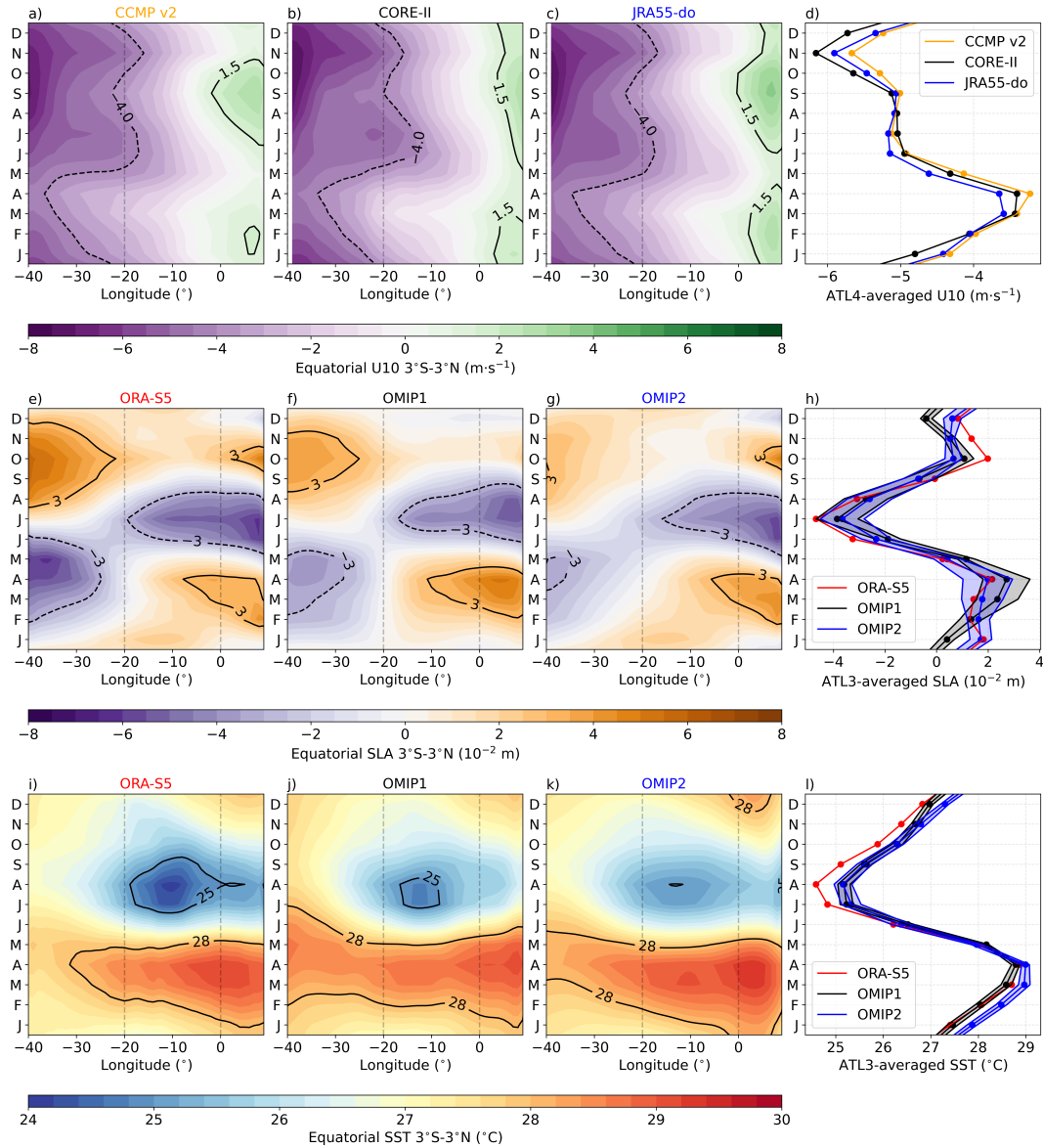
Figure 2. Hovmöller diagrams of monthly climatologies for equatorial Atlantic U10, SLA, and SST. (a) Monthly climatology of CCMP v2 U10, averaged between 3°S and 3°N and presented as a function of longitude and calendar month for the period January 1988 to December 2004. (b, c) same as (a) but for CORE-II and JRA55-do U10 over the period January 1985 to December 2004. (d) Monthly climatologies of the ATL4-averaged U10 from CCMP v2 (orange), CORE-II (black), and JRA55-do (blue). (e, f, g) Monthly climatologies of SLA in ORA-S5, OMIP1 ensemble mean, and OMIP2 ensemble mean, averaged between 3°S and 3°N, shown as a function of the longitude and calendar month for the period from January 1985 to December 2004. (h) Monthly climatologies of the ATL3-averaged SLA from ORA-S5 (red), OMIP1 (black), and OMIP2 (blue). (i, j, k, l) Same as (e, f, g, h) but for the SST.
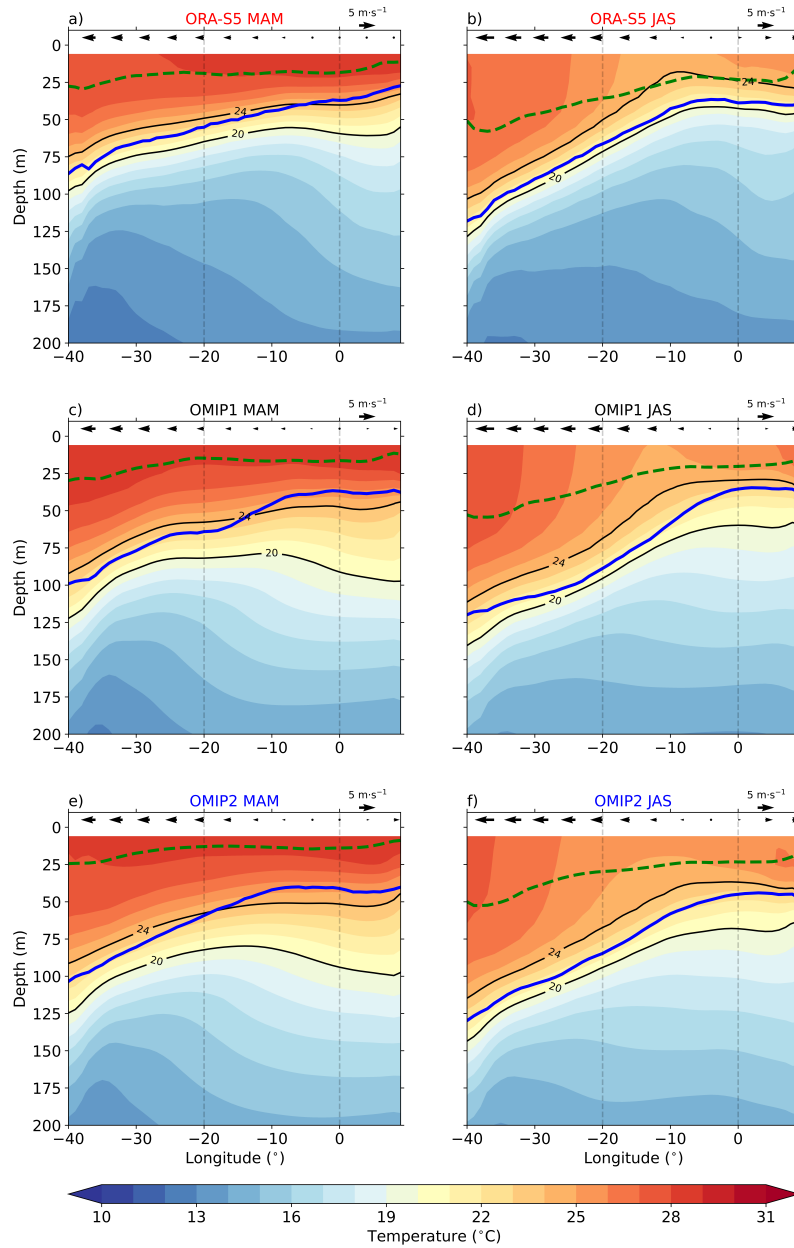
Figure 3. Upper 200 m ocean temperature for MAM (left) and JAS (right). (a, c, e) MAM upper 200 m ocean temperature in the equatorial Atlantic (40°W-9°E, 3°S-3°N) with shading, where black arrows indicate zonal wind at 10 m height, thick blue lines denote the maximum dT/dz, green dashed lines represent the mixed layer depth, and black lines indicate the depths of the 20 °C and 24 °C isotherms for ORA-S5, OMIP1 and OMIP2 ensemble means, respectively. (b, d, f) Same as (a, c, e) but for JAS. Vertical black dashed lines denote the ATL3 region.
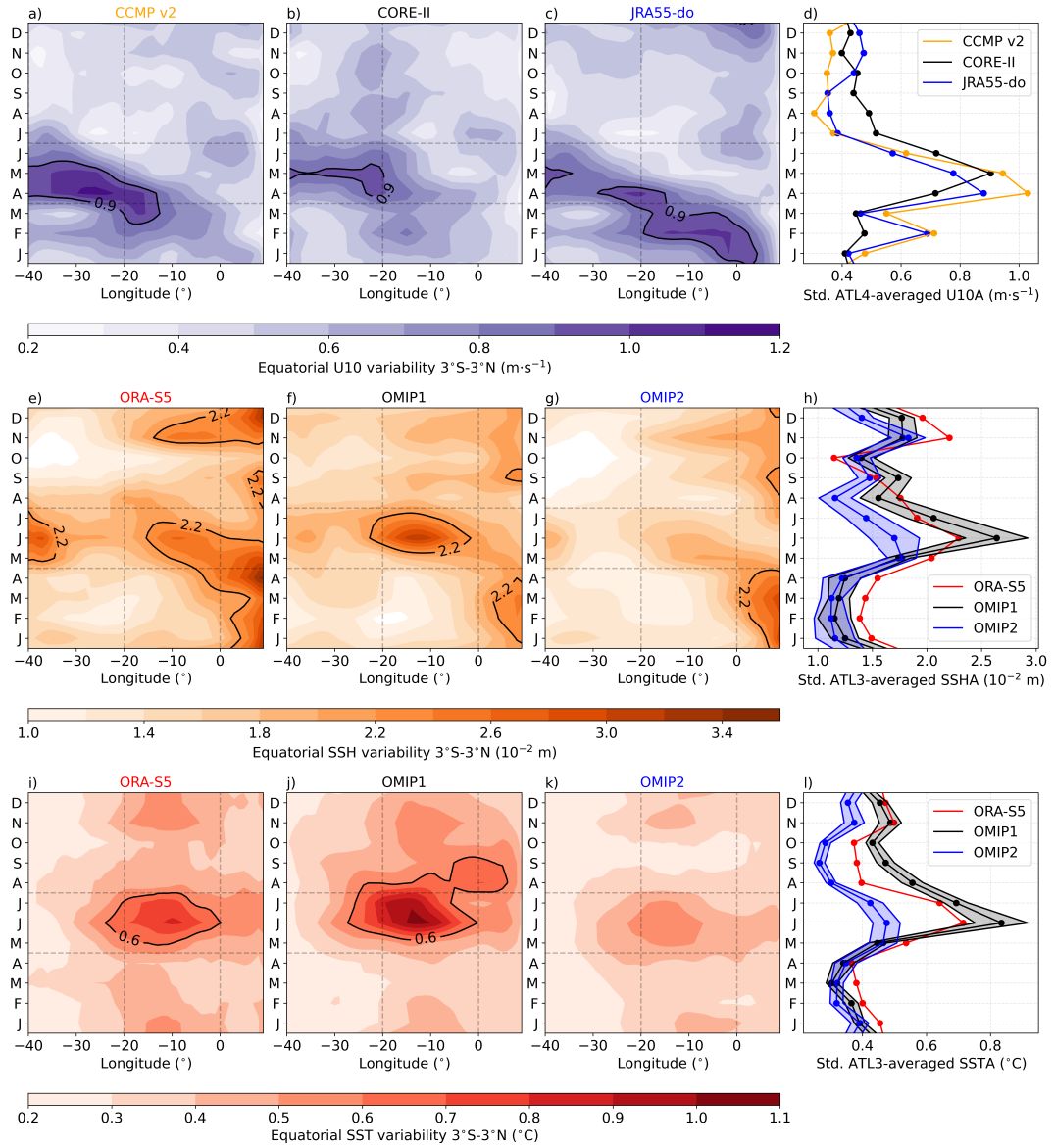
Figure 4. Same as Figure 2 but for the monthly climatological standard deviation of interannual anomalies. Vertical lines in panels a, b, c (e, f, g, i, j, k) denotes the ATL4 (ATL3) region. Horizontal lines in panels a, b, c (e, f, g, i, j, k) highlight the AMJ (MJJ) months.
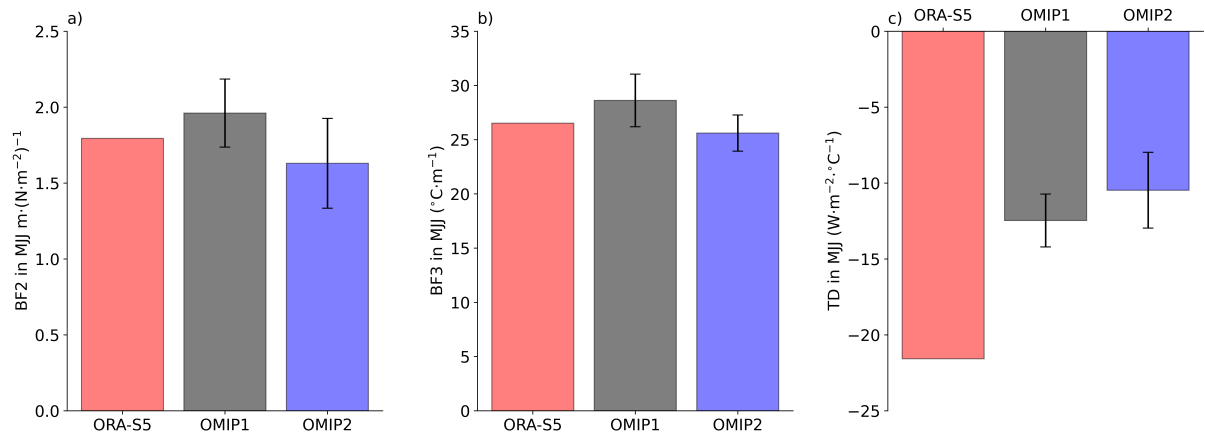
Figure 5. Bjerknes feedback components and thermal damping during MJJ over the period from January 1985 to December 2004. (a) Histogram of the BF2 in MJJ for ORA-S5 (grey), the OMIP1 ensemble (blue), and the OMIP2 ensemble (red). (b) Same as (a) but for the BF3. (c) Same as (a) but for the thermal damping (TD). Error bars are defined as $\pm$ one standard deviation of the ensemble.
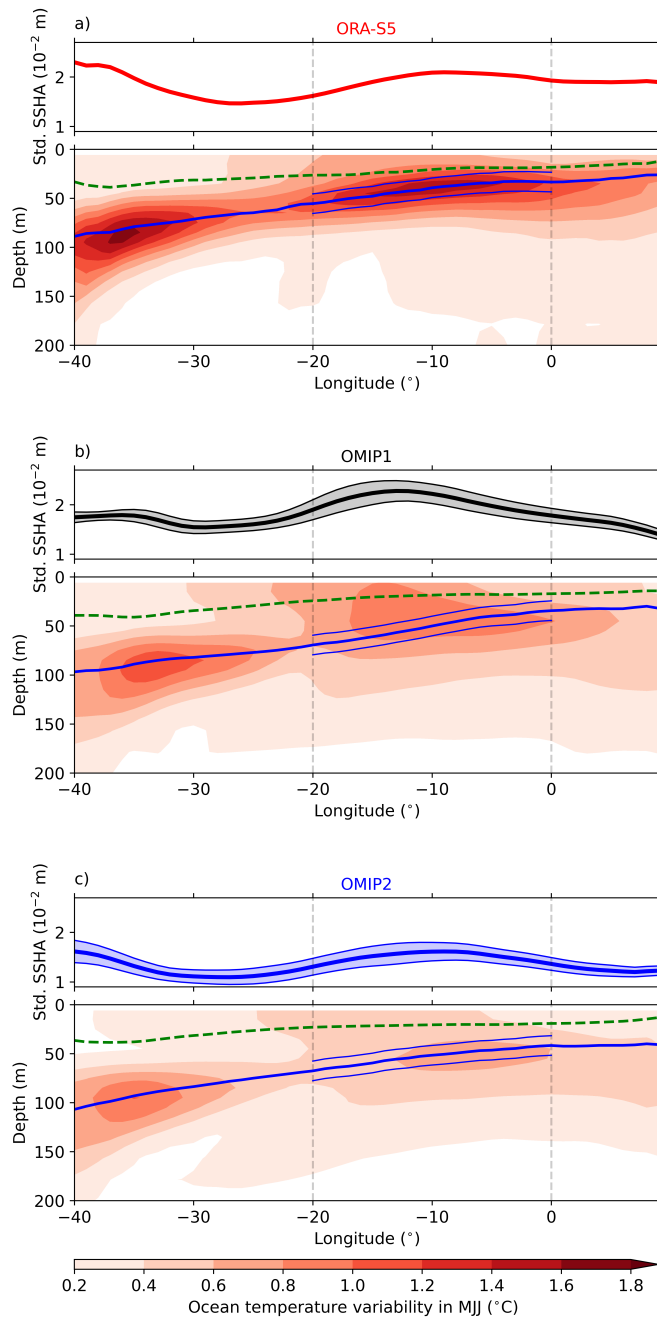
Figure 6. Equatorial Atlantic (40°W-9°E, 3°S-3°N) interannual variability of SSH and upper 200 m ocean temperature during MJJ over the period from January 1985 to December 2004 for (a) ORA-S5, (b) the OMIP1 ensemble mean, and (c) the OMIP2 ensemble mean. Thick blue lines represent the depth of maximum dT/dz, while green dashed lines denote the mixed layer depth. Thin blue lines encompass a ± 10 m range around the mean thermocline. Vertical dashed lines in black denote the ATL3 region.
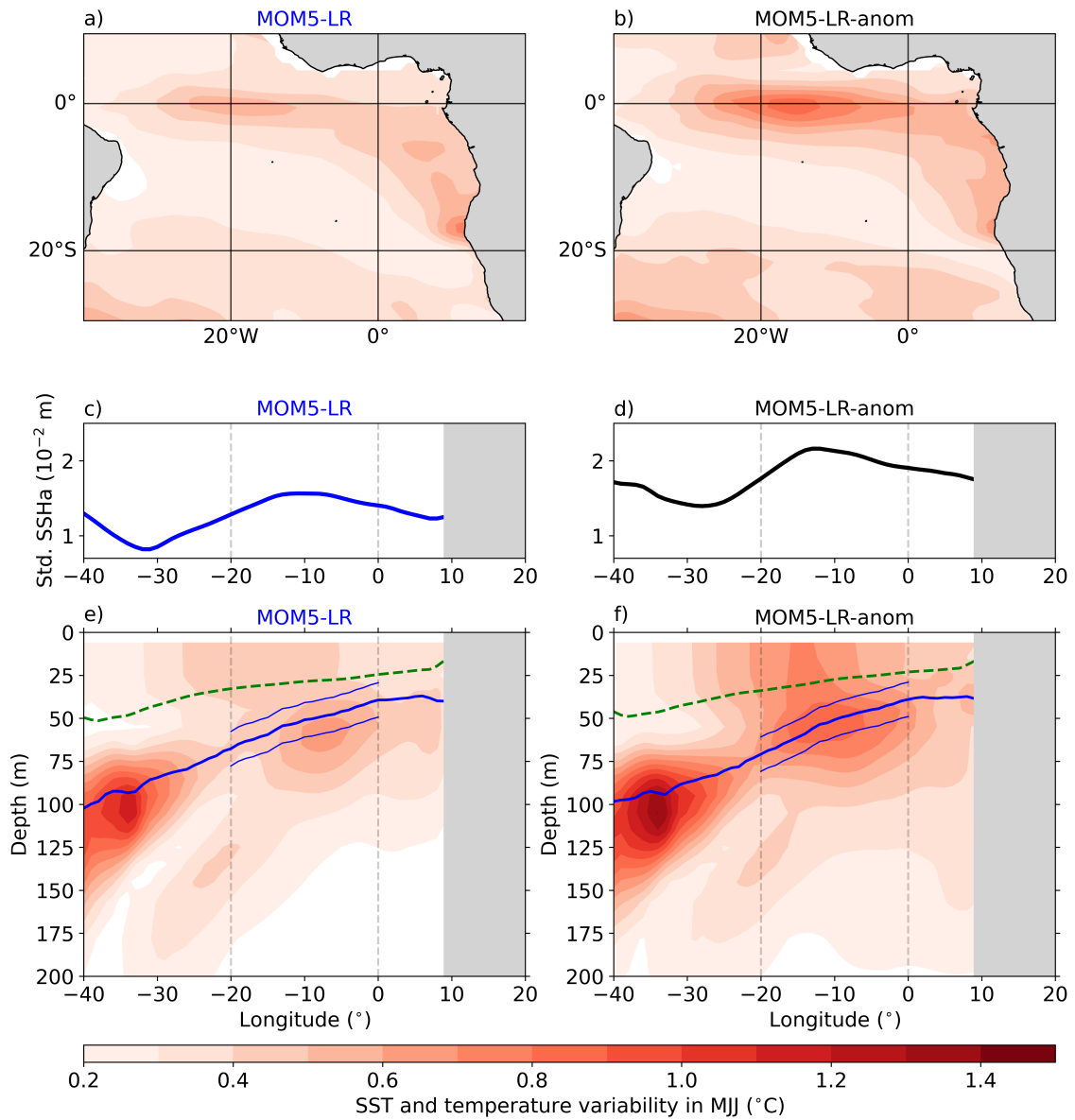
Figure 7. Interannual SST, SSH and upper 200 m temperature variability during MJJ over the period from January 1985 to December 2004. (a) Standard deviation of SST anomalies averaged over MJJ for MOM5-LR. (c) Standard deviation of SSH anomalies in the equatorial Atlantic (3°S-3°N) during MJJ for MOM5-LR. (e) Standard deviation of the equatorial Atlantic MJJ upper 200 m temperature anomalies for MOM5-LR. (b, d, f) Same as (a, c, e) but for MOM5-LR-anom. The dashed green lines represent the MLD. The solid blue lines indicate the depth of the maximum vertical temperature gradient in MJJ. Thin blue lines encompass a $\pm$ 10 m range around the mean thermocline. Vertical dashed black lines denote the ATL3 region.
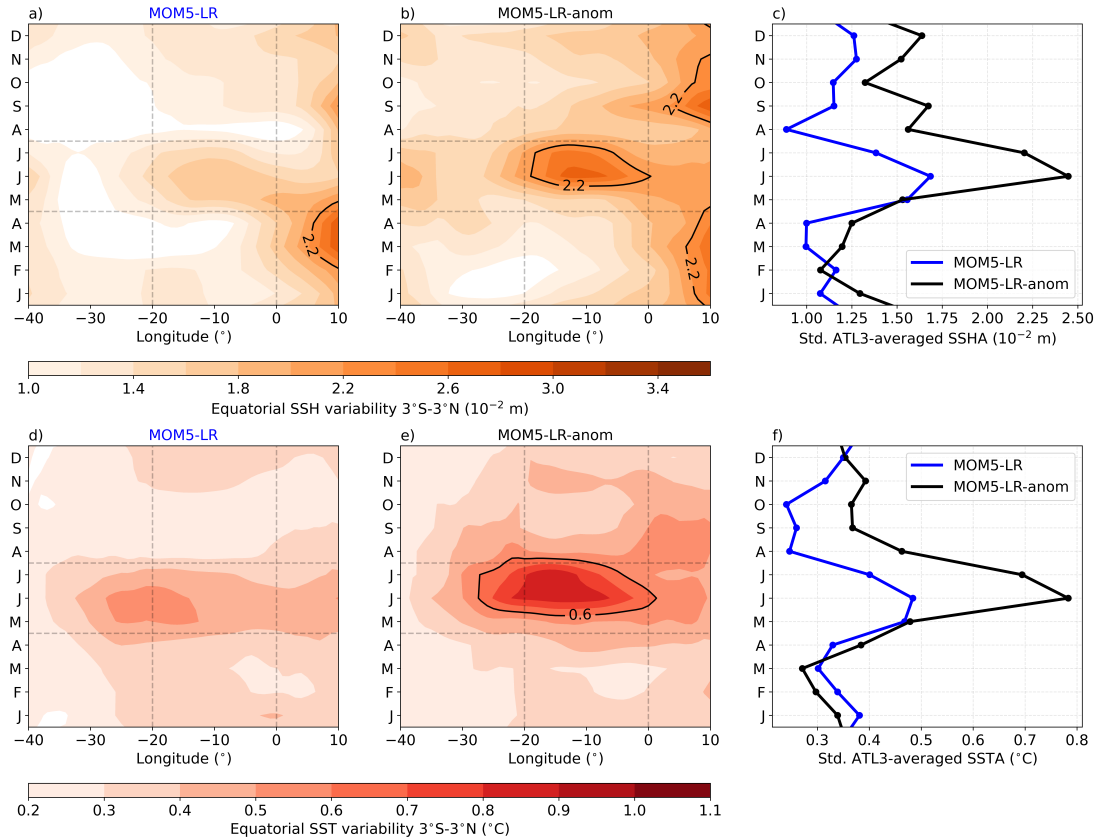
Figure 8. Hovmöller diagrams depicting the interannual variability of SSH and SST over the period from January 1985 to December 2004. (a) Monthly climatological standard deviation of the MOM5-LR SSHA, averaged between 3°S and 3°N, plotted as a function of longitude and calendar month. (b) Same as (a) but for MOM5-LR-anom. (c) Monthly climatological standard deviation of the ATL3-averaged SSHA for MOM5-LR (blue) and MOM5-LR-anom (black). (d, e, f) Same as (a, b, c) but for the SSTA.
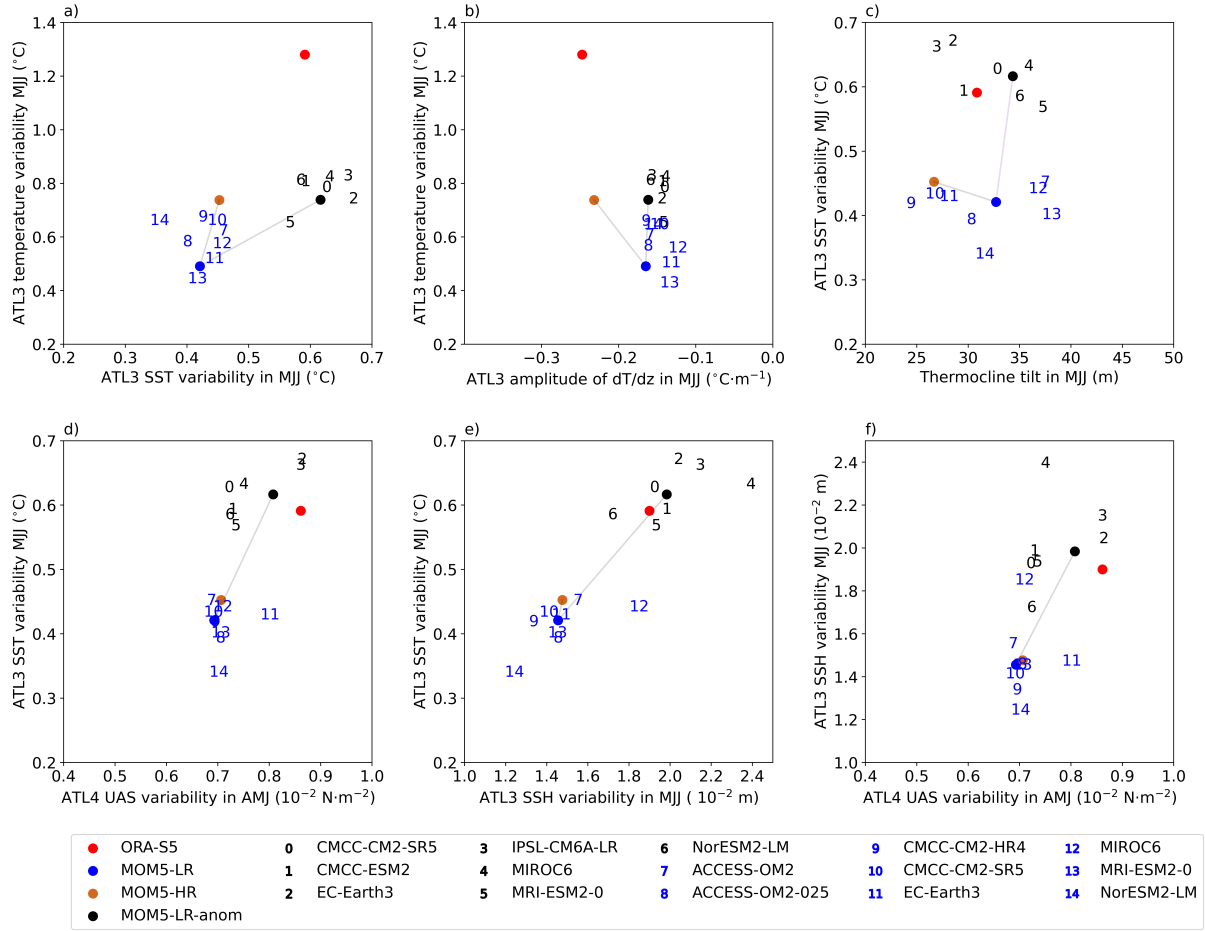
Figure 9. Scatter plots illustrating various equatorial Atlantic metrics assessed during the period January 1985 to December 2004. (a) Relationship between the standard deviation of ATL3-averaged SST anomalies in MJJ and the ATL3-averaged temperature anomalies in MJJ within ±10 m around the mean thermocline. (b) Relationship between ATL3-averaged dT/dz within ±10 m around the mean thermocline in MJJ and the ATL3-averaged temperature anomalies in MJJ within ±10 m around the mean thermocline. (c) Relationship between the equatorial Atlantic thermocline tilt in MJJ and the standard deviation of ATL3-averaged SST anomalies in MJJ. The equatorial thermocline tilt is defined as the difference between ATL4-averaged and ATL3-averaged depth of the maximum dT/dz. (d) Relationship between the standard deviation of ATL4-averaged UAS anomalies in AMJ and the standard deviation of ATL3-averaged SST anomalies in MJJ. (e) Relationship between the standard deviation of ATL3-averaged SSH anomalies in MJJ and the standard deviation of ATL3-averaged SST anomalies in MJJ. (f) Relationship between the standard deviation of ATL4-averaged UAS anomalies in MJJ and the standard deviation of ATL3-averaged SSH anomalies in MJJ. Dots are colour-coded: red, blue, brown and black dots represent ORA-S5, MOM5-LR, MOM5-HR, and MOM5-LR-anom, respectively. Black (blue) numbers denote the OMIP1 (OMIP2) models.
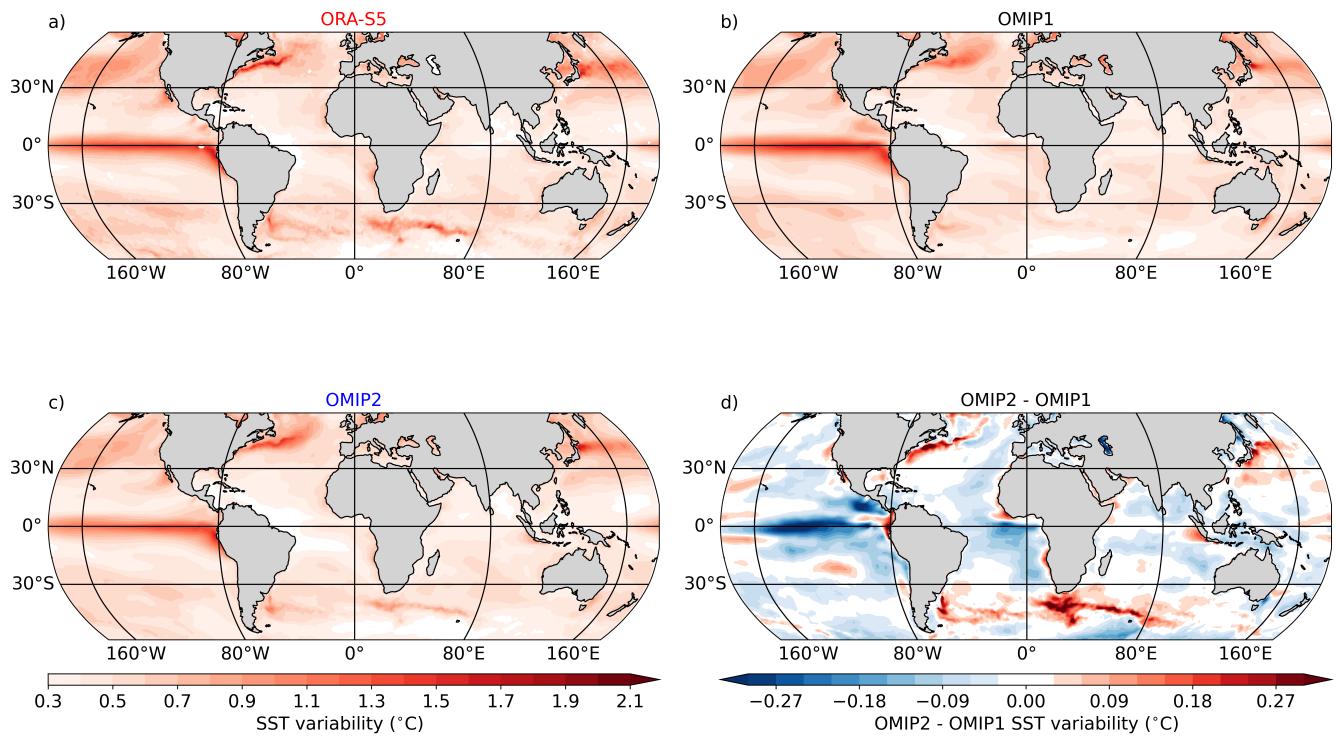
Figure 10. Standard deviation of monthly mean SST anomalies for (a) ORA-S5, (b) the OMIP1 ensemble mean, (c) the OMIP2 ensemble mean spanning from January 1985 to December 2004. (d) Difference between the OMIP2 ensemble mean minus the OMIP1 ensemble mean.

Author contributions.

AP carried out the analyses and wrote the first draft of the manuscript. RF ran the sensitivity experiments and participated in the conceptualization, editing, and reviewing of the manuscript.

Competing interests.

440   The authors declare no competing interests.

Acknowledgements. We acknowledge the infrastructure and financial support of The Abdus Salam International Center for Theoretical Physics (ICTP). We thank the two anonymous reviewers for their constructive comments that helped to improve this manuscript. We also thank the climate modelling groups for producing and making available their model output, the Earth System Grid Federation (ESGF) for archiving the data and providing access.

References

Adcroft, A., Anderson, W., Balaji, V., Blanton, C., Bushuk, M., Dufour, C. O., Dunne, J. P., Griffies, S. M., Hallberg, R., Harrison, M. J., Held, I. M., Jansen, M. F., John, J. G., Krasting, J. P., Langenhorst, A. R., Legg, S., Liang, Z., McHugh, C., Radhakrishnan, A., Reichl, B. G., Rosati, T., Samuels, B. L., Shao, A., Stouffer, R., Winton, M., Wittenberg, A. T., Xiang, B., Zadeh, N., and Zhang, R.: The GFDL Global Ocean and Sea Ice Model OM4.0: Model Description and Simulation Features, Journal of Advances in Modeling Earth Systems, 11, 3167–3211, https://doi.org/https://doi.org/10.1029/2019MS001726, 2019.

Bjerknes, J.: ATMOSPHERIC TELECONNECTIONS FROM THE EQUATORIAL PACIFIC, Monthly Weather Review, 97, 163 – 172, https://doi.org/https://doi.org/10.1175/1520-0493(1969)097<0163:ATFTEP>2.3.CO;2, 1969.

Bleck, R.: An oceanic general circulation model framed in hybrid isopycnic-Cartesian coordinates, Ocean Modelling, 4, 55–88, https://doi.org/https://doi.org/10.1016/S1463-5003(01)00012-9, 2002.

Bourlès, B., Lumpkin, R., McPhaden, M. J., Hernandez, F., Nobre, P., Campos, E., Yu, L., Planton, S., Busalacchi, A., Moura, A. D., Servain, J., and Trotte, J.: THE PIRATA PROGRAM: History, Accomplishments, and Future Directions*, Bulletin of the American Meteorological Society, 89, 1111 – 1126, https://doi.org/10.1175/2008BAMS2462.1, 2008.

Brandt, P., Caniaux, G., Bourlès, B., Lazar, A., Dengler, M., Funk, A., Hormann, V., Giordani, H., and Marin, F.: Equatorial upper-ocean dynamics and their interaction with the West African monsoon, Atmospheric Science Letters, 12, 24–30, https://doi.org/https://doi.org/10.1002/asl.287, 2011.

Brandt, P., Claus, M., Greatbatch, R. J., Kopte, R., Toole, J. M., Johns, W. E., and Böning, C. W.: Annual and Semiannual Cycle of Equatorial Atlantic Circulation Associated with Basin-Mode Resonance, Journal of Physical Oceanography, 46, 3011 – 3029, https://doi.org/10.1175/JPO-D-15-0248.1, 2016.

Burls, N. J., Reason, C. J. C., Penven, P., and Philander, S. G.: Energetics of the Tropical Atlantic Zonal Mode, Journal of Climate, 25, 7442 – 7466, https://doi.org/10.1175/JCLI-D-11-00602.1, 2012.

C3S: Sea level gridded data from satellite observations for the global ocean from 1993 to present, Tech. rep., Copernicus Climate Change Service (C3S) Climate Data Store (CDS), 10.24381/cds.4c328c78, 2018.

Caniaux, G., Giordani, H., Redelsperger, J.-L., Guichard, F., Key, E., and Wade, M.: Coupling between the Atlantic cold tongue and the West African monsoon in boreal spring and summer, Journal of Geophysical Research: Oceans, 116, https://doi.org/https://doi.org/10.1029/2010JC006570, 2011.

Cassou, C., Terray, L., and Phillips, A. S.: Tropical Atlantic Influence on European Heat Waves, Journal of Climate, 18, 2805 – 2811, https://doi.org/10.1175/JCLI3506.1, 2005.

Chenillat, F., Illig, S., Jouanno, J., Awo, F. M., Alory, G., and Brehmer, P.: How do Climate Modes Shape the Chlorophyll-a Interannual Variability in the Tropical Atlantic?, Geophysical Research Letters, 48, e2021GL093 769, https://doi.org/https://doi.org/10.1029/2021GL093769, e2021GL093769 2021GL093769, 2021.

Crespo, L. R., Prigent, A., Keenlyside, N., Koseki, S., Svendsen, L., Richter, I., and Sánchez-Gómez, E.: Weakening of the Atlantic Niño variability under global warming, Nature Climate Change, 12, 822–827, https://doi.org/10.1038/s41558-022-01453-y, 2022.

Davey, M., Huddleston, M., Sperber, K., Braconnot, P., Bryan, F., Chen, D., Colman, R., Cooper, C., Cubasch, U., Delecluse, P., DeWitt, D., Fairhead, L., Flato, G., Gordon, C., Hogan, T., Ji, M., Kimoto, M., Kitoh, A., Knutson, T., Latif, M., Le Treut, H., Li, T., Manabe, S., Mechoso, C., Meehl, G., Power, S., Roeckner, E., Terray, L., Vintzileos, A., Voss, R., Wang, B., Washington, W., Yoshikawa, I., Yu, J.,

Yukimoto, S., and Zebiak, S.: STOIC: a study of coupled model climatology and variability in tropical ocean regions, Climate Dynamics, 18, 403–420, https://doi.org/10.1007/s00382-001-0188-6, 2002.

Deppenmeier, A.-L., Haarsma, R. J., and Hazeleger, W.: The Bjerknes feedback in the tropical Atlantic in CMIP5 models, Climate Dynamics, 47, 2691–2707, https://doi.org/10.1007/s00382-016-2992-z, 2016.

485 Ding, H., Keenlyside, N. S., and Latif, M.: Seasonal cycle in the upper equatorial Atlantic Ocean, Journal of Geophysical Research: Oceans, 114, https://doi.org/https://doi.org/10.1029/2009JC005418, 2009.

Dippe, T., Lübbecke, J. F., and Greatbatch, R. J.: A Comparison of the Atlantic and Pacific Bjerknes Feedbacks: Seasonality, Symmetry, and Stationarity, Journal of Geophysical Research: Oceans, 124, 2374–2403, https://doi.org/https://doi.org/10.1029/2018JC014700, 2019.

Farneti, R.: Output files for MOM5 driven by JRA55-do at 1-degree and 0.25-degree horizontal resolution,
490 https://doi.org/10.5281/zenodo.11047949, 2024.

Farneti, R., Stiz, A., and Ssebandeke, J. B.: Improvements and persistent biases in the southeast tropical Atlantic in CMIP models, npj Climate and Atmospheric Science, 5, 42, https://doi.org/10.1038/s41612-022-00264-4, 2022.

Folland, C. K., Palmer, T. N., and Parker, D. E.: Sahel rainfall and worldwide sea temperatures, 1901–85, Nature, 320, 602–607, https://doi.org/10.1038/320602a0, 1986.

495 Fox-Kemper, B., Ferrari, R., and Hallberg, R.: Parameterization of Mixed Layer Eddies. Part I: Theory and Diagnosis, Journal of Physical Oceanography, 38, 1145 – 1165, https://doi.org/https://doi.org/10.1175/2007JPO3792.1, 2008.

Fox-Kemper, B., Danabasoglu, G., Ferrari, R., Griffies, S., Hallberg, R., Holland, M., Maltrud, M., Peacock, S., and Samuels, B.: Parameterization of mixed layer eddies. III: Implementation and impact in global ocean climate simulations, Ocean Modelling, 39, 61–78, https://doi.org/https://doi.org/10.1016/j.ocemod.2010.09.002, modelling and Understanding the Ocean Mesoscale and Submesoscale,
500 2011.

Gent, P. R. and Mcwilliams, J. C.: Isopycnal Mixing in Ocean Circulation Models, Journal of Physical Oceanography, 20, 150 – 155, https://doi.org/https://doi.org/10.1175/1520-0485(1990)020<0150:IMIOCM>2.0.CO;2, 1990.

Gent, P. R., Willebrand, J., McDougall, T. J., and McWilliams, J. C.: Parameterizing Eddy-Induced Tracer Transports in Ocean Circulation Models, Journal of Physical Oceanography, 25, 463 – 474, https://doi.org/https://doi.org/10.1175/1520-
505 0485(1995)025<0463:PEITTI>2.0.CO;2, 1995.

Griffies, S.: Elements of MOM4p1, GFDL Ocean Group Tech. Rep. 6, 6, 2009.

Griffies, S. M.: The Gent–McWilliams Skew Flux, Journal of Physical Oceanography, 28, 831 – 841, https://doi.org/https://doi.org/10.1175/1520-0485(1998)028<0831:TGMSF>2.0.CO;2, 1998.

Griffies, S. M.: Elements of the Modular Ocean Model (MOM) (2012 Release), GFDL Ocean Group Technical Report No.7, NOAA/Geo-
510 physical Fluid Dynamics Laboratory, 618 + xiii pages, 2012.

Griffies, S. M., Biastoch, A., Böning, C., Bryan, F., Danabasoglu, G., Chassignet, E. P., England, M. H., Gerdes, R., Haak, H., Hallberg, R. W., Hazeleger, W., Jungclaus, J., Large, W. G., Madec, G., Pirani, A., Samuels, B. L., Scheinert, M., Gupta, A. S., Severijns, C. A., Simmons, H. L., Treguier, A. M., Winton, M., Yeager, S., and Yin, J.: Coordinated Ocean-ice Reference Experiments (COREs), Ocean Modelling, 26, 1–46, https://doi.org/https://doi.org/10.1016/j.ocemod.2008.08.007, 2009.

515 Griffies, S. M., Danabasoglu, G., Durack, P. J., Adcroft, A. J., Balaji, V., Böning, C. W., Chassignet, E. P., Curchitser, E., Deshayes, J., Drange, H., Fox-Kemper, B., Gleckler, P. J., Gregory, J. M., Haak, H., Hallberg, R. W., Heimbach, P., Hewitt, H. T., Holland, D. M., Ilyina, T., Jungclaus, J. H., Komuro, Y., Krasting, J. P., Large, W. G., Marsland, S. J., Masina, S., McDougall, T. J., Nurser, A. J. G., Orr, J. C., Pirani, A., Qiao, F., Stouffer, R. J., Taylor, K. E., Treguier, A. M., Tsujino, H., Uotila, P., Valdivieso, M., Wang, Q., Winton, M.,

and Yeager, S. G.: OMIP contribution to CMIP6: experimental and diagnostic protocol for the physical component of the Ocean Model
Intercomparison Project, Geoscientific Model Development, 9, 3231–3296, https://doi.org/10.5194/gmd-9-3231-2016, 2016.

Griffies, S. M., Adcroft, A., and Hallberg, R. W.: A Primer on the Vertical Lagrangian-Remap Method in Ocean Models Based
on Finite Volume Generalized Vertical Coordinates, Journal of Advances in Modeling Earth Systems, 12, e2019MS001954,
https://doi.org/https://doi.org/10.1029/2019MS001954, e2019MS001954 10.1029/2019MS001954, 2020.

Hirst, A. C. and Hastenrath, S.: Atmosphere-Ocean Mechanisms of Climate Anomalies in the Angola-Tropical Atlantic Sector, Journal of
Physical Oceanography, 13, 1146 – 1157, https://doi.org/https://doi.org/10.1175/1520-0485(1983)013<1146:AOMOCA>2.0.CO;2, 1983.

Illig, S., Dewitte, B., Ayoub, N., du Penhoat, Y., Reverdin, G., De Mey, P., Bonjean, F., and Lagerloef, G. S. E.: Interannual long equatorial
waves in the tropical Atlantic from a high-resolution ocean general circulation model experiment in 1981–2000, Journal of Geophysical
Research: Oceans, 109, https://doi.org/https://doi.org/10.1029/2003JC001771, 2004.

Jouanno, J., Hernandez, O., and Sanchez-Gomez, E.: Equatorial Atlantic interannual variability and its relation to dynamic and thermody-
namic processes, Earth System Dynamics, 8, 1061–1069, https://doi.org/10.5194/esd-8-1061-2017, 2017.

Kanamitsu, M., Ebisuzaki, W., Woollen, J., Yang, S.-K., Hnilo, J. J., Fiorino, M., and Potter, G. L.: NCEP–DOE AMIP-II Reanalysis (R-2),
Bulletin of the American Meteorological Society, 83, 1631 – 1644, https://doi.org/https://doi.org/10.1175/BAMS-83-11-1631, 2002.

Keenlyside, N. S. and Latif, M.: Understanding Equatorial Atlantic Interannual Variability, Journal of Climate, 20, 131 – 142,
https://doi.org/https://doi.org/10.1175/JCLI3992.1, 2007.

Kucharski, F., Bracco, A., Yoo, J. H., and Molteni, F.: Atlantic forced component of the Indian monsoon interannual variability, Geophysical
Research Letters, 35, https://doi.org/https://doi.org/10.1029/2007GL033037, 2008.

Large, W. G. and Yeager, S. G.: The global climatology of an interannually varying air–sea flux data set, Climate Dynamics, 33, 341–364,
https://doi.org/10.1007/s00382-008-0441-3, 2009.

Large, W. G., McWilliams, J. C., and Doney, S. C.: Oceanic vertical mixing: A review and a model with a nonlocal boundary layer parame-
terization, Reviews of Geophysics, 32, 363–403, https://doi.org/https://doi.org/10.1029/94RG01872, 1994.

Lübbecke, J. F. and McPhaden, M. J.: Symmetry of the Atlantic Niño mode, Geophysical Research Letters, 44, 965–973,
https://doi.org/https://doi.org/10.1002/2016GL071829, 2017.

Lübbecke, J. F., Rodríguez-Fonseca, B., Richter, I., Martín-Rey, M., Losada, T., Polo, I., and Keenlyside, N. S.:
Equatorial Atlantic variability—Modes, mechanisms, and global teleconnections, WIREs Climate Change, 9, e527,
https://doi.org/https://doi.org/10.1002/wcc.527, 2018.

Mears, C. A., Scott, J., Wentz, F. J., Ricciardulli, L., Leidner, S. M., Hoffman, R., and Atlas, R.: A Near-Real-Time Version of the Cross-
Calibrated Multiplatform (CCMP) Ocean Surface Wind Velocity Data Set, Journal of Geophysical Research: Oceans, 124, 6997–7010,
https://doi.org/https://doi.org/10.1029/2019JC015367, 2019.

Nobre, P. and Shukla, J.: Variations of Sea Surface Temperature, Wind Stress, and Rainfall over the Tropical Atlantic and South America,
Journal of Climate, 9, 2464 – 2479, https://doi.org/https://doi.org/10.1175/1520-0442(1996)009<2464:VOSSTW>2.0.CO;2, 1996.

Okumura, Y. and Xie, S.-P.: Some Overlooked Features of Tropical Atlantic Climate Leading to a New Niño-Like Phenomenon, Journal of
Climate, 19, 5859 – 5874, https://doi.org/10.1175/JCLI3928.1, 2006.

Philander, S. G. H. and Pacanowski, R. C.: A model of the seasonal cycle in the tropical Atlantic Ocean, Journal of Geophysical Research:
Oceans, 91, 14 192–14 206, https://doi.org/https://doi.org/10.1029/JC091iC12p14192, 1986.

Prigent, A., Imbol Koungue, R. A., Imbol Nkwinkwa, A. S. N., Beobide-Arsuaga, G., and Farneti, R.: Uncertainty on Atlantic Niño Variability
Projections, Geophysical Research Letters, 50, e2023GL105 000, https://doi.org/https://doi.org/10.1029/2023GL105000, 2023a.

Prigent, A., Imbol Koungue, R. A., Lübbecke, J. F., Brandt, P., Harlaß, J., and Latif, M.: Future weakening of southeastern tropical Atlantic Ocean interannual sea surface temperature variability in a global climate model, Climate Dynamics, https://doi.org/10.1007/s00382-023-07007-y, 2023b.

560 Prodhomme, C., Voldoire, A., Exarchou, E., Deppenmeier, A.-L., García-Serrano, J., and Guemas, V.: How Does the Seasonal Cycle Control Equatorial Atlantic Interannual Variability?, Geophysical Research Letters, 46, 916–922, https://doi.org/https://doi.org/10.1029/2018GL080837, 2019.

Reynolds, R. W., Rayner, N. A., Smith, T. M., Stokes, D. C., and Wang, W.: An Improved In Situ and Satellite SST Analysis for Climate, Journal of Climate, 15, 1609 – 1625, https://doi.org/https://doi.org/10.1175/1520-0442(2002)015<1609:AIISAS>2.0.CO;2, 2002.

565 Richter, I. and Tokinaga, H.: An overview of the performance of CMIP6 models in the tropical Atlantic: mean state, variability, and remote impacts, Climate Dynamics, 55, 2579–2601, https://doi.org/10.1007/s00382-020-05409-w, 2020.

Richter, I., Xie, S.-P., Wittenberg, A. T., and Masumoto, Y.: Tropical Atlantic biases and their relation to surface wind stress and terrestrial precipitation, Climate Dynamics, 38, 985–1001, https://doi.org/10.1007/s00382-011-1038-9, 2012.

Rodríguez-Fonseca, B., Polo, I., García-Serrano, J., Losada, T., Mohino, E., Mechoso, C. R., and Kucharski, F.: Are Atlantic Niños enhancing 570 Pacific ENSO events in recent decades?, Geophysical Research Letters, 36, https://doi.org/https://doi.org/10.1029/2009GL040048, 2009.

Saha, S., Moorthi, S., Pan, H.-L., Wu, X., Wang, J., Nadiga, S., Tripp, P., Kistler, R., Woollen, J., Behringer, D., Liu, H., Stokes, D., Grumbine, R., Gayno, G., Wang, J., Hou, Y.-T., ya Chuang, H., Juang, H.-M. H., Sela, J., Iredell, M., Treadon, R., Kleist, D., Delst, P. V., Keyser, D., Derber, J., Ek, M., Meng, J., Wei, H., Yang, R., Lord, S., van den Dool, H., Kumar, A., Wang, W., Long, C., Chelliah, M., Xue, Y., Huang, B., Schemm, J.-K., Ebisuzaki, W., Lin, R., Xie, P., Chen, M., Zhou, S., Higgins, W., Zou, C.-Z., Liu, Q., Chen, Y., Han, Y., 575 Cucurull, L., Reynolds, R. W., Rutledge, G., and Goldberg, M.: The NCEP Climate Forecast System Reanalysis, Bulletin of the American Meteorological Society, 91, 1015 – 1058, https://doi.org/https://doi.org/10.1175/2010BAMS3001.1, 2010.

Servain, J., Picaut, J., and Merle, J.: Evidence of Remote Forcing in the Equatorial Atlantic Ocean, Journal of Physical Oceanography, 12, 457 – 463, https://doi.org/https://doi.org/10.1175/1520-0485(1982)012<0457:EORFIT>2.0.CO;2, 1982.

Servain, J., Busalacchi, A. J., McPhaden, M. J., Moura, A. D., Reverdin, G., Vianna, M., and Zebiak, S. E.: A Pilot Research Moored Array 580 in the Tropical Atlantic (PIRATA), Bulletin of the American Meteorological Society, 79, 2019 – 2032, https://doi.org/10.1175/1520-0477(1998)079<2019:APRMAI>2.0.CO;2, 1998.

Taboada, F. G., Stock, C. A., Griffies, S. M., Dunne, J., John, J. G., Small, R. J., and Tsujino, H.: Surface winds from atmospheric reanalysis lead to contrasting oceanic forcing and coastal upwelling patterns, Ocean Modelling, 133, 79–111, https://doi.org/https://doi.org/10.1016/j.ocemod.2018.11.003, 2019.

585 Treguier, A. M., de Boyer Montégut, C., Bozec, A., Chassignet, E. P., Fox-Kemper, B., McC. Hogg, A., Iovino, D., Kiss, A. E., Le Sommer, J., Li, Y., Lin, P., Lique, C., Liu, H., Serazin, G., Sidorenko, D., Wang, Q., Xu, X., and Yeager, S.: The mixed-layer depth in the Ocean Model Intercomparison Project (OMIP): impact of resolving mesoscale eddies, Geoscientific Model Development, 16, 3849–3872, https://doi.org/10.5194/gmd-16-3849-2023, 2023.

Tsujino, H., Urakawa, S., Nakano, H., Small, R. J., Kim, W. M., Yeager, S. G., Danabasoglu, G., Suzuki, T., Bamber, J. L., Bentsen, M., 590 Böning, C. W., Bozec, A., Chassignet, E. P., Curchitser, E., Boeira Dias, F., Durack, P. J., Griffies, S. M., Harada, Y., Ilicak, M., Josey, S. A., Kobayashi, C., Kobayashi, S., Komuro, Y., Large, W. G., Le Sommer, J., Marsland, S. J., Masina, S., Scheinert, M., Tomita, H., Valdivieso, M., and Yamazaki, D.: JRA-55 based surface dataset for driving ocean–sea-ice models (JRA55-do), Ocean Modelling, 130, 79–139, https://doi.org/https://doi.org/10.1016/j.ocemod.2018.07.002, 2018.

Tsujino, H., Urakawa, L. S., Griffies, S. M., Danabasoglu, G., Adcroft, A. J., Amaral, A. E., Arsouze, T., Bentsen, M., Bernardello, R., Böning, C. W., Bozec, A., Chassignet, E. P., Danilov, S., Dussin, R., Exarchou, E., Fogli, P. G., Fox-Kemper, B., Guo, C., Ilicak, M., Iovino, D., Kim, W. M., Koldunov, N., Lapin, V., Li, Y., Lin, P., Lindsay, K., Liu, H., Long, M. C., Komuro, Y., Marsland, S. J., Masina, S., Nummelin, A., Rieck, J. K., Ruprich-Robert, Y., Scheinert, M., Sicardi, V., Sidorenko, D., Suzuki, T., Tatebe, H., Wang, Q., Yeager, S. G., and Yu, Z.: Evaluation of global ocean–sea-ice model simulations based on the experimental protocols of the Ocean Model Intercomparison Project phase 2 (OMIP-2), Geoscientific Model Development, 13, 3643–3708, https://doi.org/10.5194/gmd-13-3643-2020, 2020.

Wahl, S., Latif, M., Park, W., and Keenlyside, N.: On the Tropical Atlantic SST warm bias in the Kiel Climate Model, Climate Dynamics, 36, 891–906, https://doi.org/10.1007/s00382-009-0690-9, 2011.

Wen, C., Xue, Y., Kumar, A., Behringer, D., and Yu, L.: How do uncertainties in NCEP R2 and CFSR surface fluxes impact tropical ocean simulations?, Climate Dynamics, 49, 3327–3344, https://doi.org/10.1007/s00382-016-3516-6, 2017.

Xie, S.-P. and Carton, J. A.: Tropical Atlantic Variability: Patterns, Mechanisms, and Impacts, pp. 121–142, American Geophysical Union (AGU), https://doi.org/https://doi.org/10.1029/147GM07, 2004.

Zebiak, S. E.: Air–Sea Interaction in the Equatorial Atlantic Region, Journal of Climate, 6, 1567 – 1586, https://doi.org/https://doi.org/10.1175/1520-0442(1993)006<1567:AIITEA>2.0.CO;2, 1993.

Zuo, H., Balmaseda, M. A., Tietsche, S., Mogensen, K., and Mayer, M.: The ECMWF operational ensemble reanalysis–analysis system for ocean and sea ice: a description of the system and assessment, Ocean Science, 15, 779–808, https://doi.org/10.5194/os-15-779-2019, 2019.